Contract No.:

This manuscript has been authored by Savannah River Nuclear Solutions (SRNS), LLC under Contract No. DE-AC09-08SR22470 with the U.S. Department of Energy (DOE) Office of Environmental Management (EM).

Electronic Structure of Actinide Oxides

Introduction

Understanding the structure, properties, and reactivity of actinide oxides is central not only from a fundamental standpoint but also technological given the dominant role they play in nuclear applications. Uranium, for example, is extracted from ores consisting primarily of the mineral uraninite or pitchblende deposits (UO_2, U_3O_8, and UO_3 in varying proportions) and through the nuclear fuel cycle is converted to UO_2.[1] Uranium dioxide has been the main fuel component in light water nuclear reactors where Pu and Np are produced as a by-product of nuclear power. When considerable amounts of high-level radioactive waste created long-term storage issues, it was soon realized that small amounts of PuO_2 blended with large amounts of natural or depleted UO_2, or mixed oxide (MOX) fuels exhibit both physical characteristics and reactor performance as original UO_2 fuel.[2] Now, Np as well as other minor actinides such as Am and Cm are being considered for advanced nuclear fuels.[3] The stability of PuO_2 has been a key factor in the long-term storage of plutonium.[4] Beyond the nuclear fuel cycle, $^{237}NpO_2$ is a target material irradiated to produce $^{238}PuO_2$, which is used to fabricate radioisotope thermoelectric generators for satellite and space probe applications. Additional advances for this concept include studies of U-doped AmO_2 as a heat source for radioisotope-based energy supply systems.[5] In catalysis, uranium oxides have also shown to be promising catalysts in reactions of hydrogen or syn-gas production, Fischer-Tropsch process, partial oxidation, cracking, motor fuel hydrotreatment, and purification of exhaust gases for environmental protection.[6]

Evaluating the actinide oxide physicochemical properties allows for the development and expansion of not only new processing and storage strategies but also future areas such as catalysis. Underneath their binary formula belies a complex chemistry wherein a number of oxidation states and polymorphs complicate the overall structural features which affect materials properties. The best descriptions include both *ab initio* calculations and experimental techniques to provide a fuller, more accurate picture of the electronic structure.[7] However, their study faces several challenges. Polymorphs are often unstable and general toxicity adds another source of complication; experiments are further limited by low abundance and difficulties isolating material. Theoretical chemistry has emerged as a powerful tool capable of determining and predicting properties especially across the series, but the implementation is not simple. Electronic structure calculations based on local spin-density approximation (LSDA) to density functional theory (DFT) often fail due to the relativistic influences and highly correlated nature of these materials. To circumvent these problems, other methods have been developed to calculate high correlated materials: self-interaction correction methods (SIC),[8] modified density functional theory (DFT+U),[8-9] dynamic mean field theory (DMFT),[10] and screened hybrid density functional theory (HSE).[11]

Of the oxides, the dioxides represent the most complete analysis of the actinide series; of the elements, the most comprehensive study of structure-property relationships has been performed for the uranium oxides; and of the methods, DFT + U has been able to accurately reproduce the known properties of the actinide oxides at a reasonable computational cost. This review will provide an overview of the electronic

structure calculations of the actinide oxides based on both performance of various functionals and modeling of various polymorphs, in particular for the uranium oxides.

Actinide Dioxides

The actinide dioxides are insulators and crystalize in the fluorite or CaF_2 structure with $Fm\bar{3}m$ symmetry, as shown in Figure 1. [7b, 12] The metal centers form the cubic close packing (ccp) arrangement, i.e., these ions occupy the corner and center of each face of the cube. The oxygen ions occupy tetrahedral sites with a coordination number of 4 and each metal center is eight-coordinate. The cell parameters can be found in Table 1, in comparison with optimized data, with Figure 2 illustrating the linear dependence of the cell parameter to ionic radius of the actinide cation.

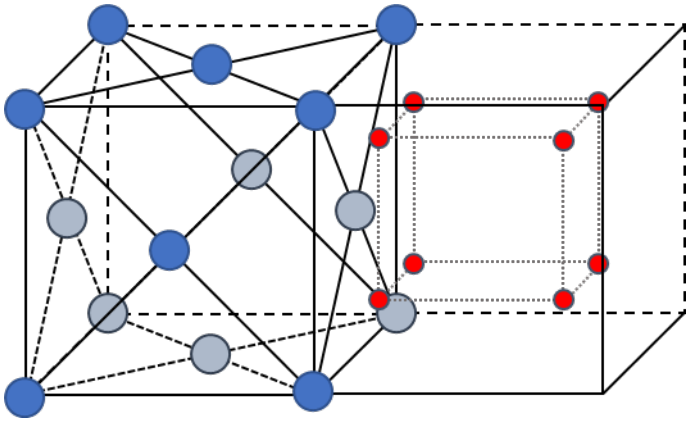

Figure 1. AnO_2 fluorite (CaF_2) structure; the actinide (left) sublattice is fcc while the oxygen (right) sublattice is primitive cubic.

Table 1. Comparison of optimized lattice constant in angstroms (Å) for actinide dioxides with experiment.

Compound	Method	a (Å)		B (GPa)		Δ_{gap} (eV)		E_{FM-AFM} (meV)
		FM	AFM	FM	AFM	FM	AFM	
ThO_2	PBE[13]	5.615		192		4.52		--
	PBE+U[14]	5.671		--		4.7		--
	AM05/PBE-Sol [15]	5.637		201		4.63		--
	HSE-gaussian[13]	5.595		207		6.22		--
	HSE-VASP[14]	5.580		--		6.0		
	HSE+SOC[14]	5.580		--		5.8		--
	Expt[16 17 12c]	5.597		198		6		--
PaO_2	PBE[13]	5.479	5.466	202	205	0	0	-6
	PBE+U[14]	5.544		--		0		--
	HSE-gaussian[13]	5.517	5.518	208	207	0.67	1.36	-4
	HSE-VASP[14]	5.483	5.501	--	--	--	1.2	+250
	HSE+SOC[14]	5.494	5.499	--	--	--	1.5	+20
	Expt[18]	5.505		--		--		--

UO_2	LSDA[13]	5.317	5.289	239	216	0	0	-98
	PBE[13]	5.425	5.445	206	186	0	0	-123
	PBE+U[13]	5.455	5.454	220	219	2.23	3.13	+2
	PBE+U[14]	5.568		--		2.3		--
	DFT+U[15]	--	5.474	--	210	--	2.06	--
	AM05/PBE-Sol[15]							
	HSE-gaussian[13]	5.463	5.463	226	218	1.56	2.39	+7
	HSE-VASP[14]	5.418	5.458	--	--	--	2.4	+190
	HSE+SOC[14]	5.457	5.457	--	--		2.4	+100
	SIC-LSD U^{5+}[19]	5.40		219		0		--
	SIC-LSD U^{4+}[19]	5.47		219		2.6		--
	DMFT[20]	--		--		1.9		--
	Expt[16 12c, 21]	5.470		207		2.1		>0
NpO_2	PBE[13]	5.400	5.434	186	194	0	0.16	-116
	PBE+U[14]	5.498		--		2.6		--
	DFT+U[15]	5.448		214		3.08		--
	HSE-gaussian[13]	5.424	5.424	225	224	2.84	3.08	-5
	HSE-VASP[14]	5.411	5.412	--	--	--	2.4	-120
	HSE+SOC[14]	5.418	5.418	--	--	--	2.4	150
	SIC-LSD[19]	5.460		217		2.3		--
	DMFT[20]	--		--		2.5		--
	Expt[16 22]	5.434		200		--		--
PuO_2	LSDA[13]	5.278	5.285	229	222	0	0	-310
	PBE[13]	5.399	5.412	189	182	0	0	-259
	PBE+U[13]	5.387	5.385	221	221	2.40	3.39	+14
	PBE+U[14]	5.465		--		1.6		--
	AM05/PBE-Sol [15]	5.411		217		2.81		--
	HSE-gaussian[13]	5.398	5.396	221	220	1.68	2.64	+14
	HSE-VASP[14]	5.378	5.383	--	--	--	2.4	+150
	HSE+SOC[14]	5.373	5.379	--	--	--	2.6	+10
	SIC-LSD[19]	5.440		214		1.2		--
	DMFT[20]	--		--		~3.5		
	Expt[16 12c, 23]	5.395		178		2.8		>0
AmO_2	PBE[13]	5.404	5.402	180	178	0	0	-183
	PBE+U[14]	5.425		--		0		--
	DFT+U[15]	5.379		196		1.31		
	AM05/PBE-Sol[15]							
	HSE-gaussian[13]	5.370	5.369	214	217	1.04	1.60	-16
	HSE-VASP[14]	5.362	5.375	--	--	--	1.5	+150
	HSE+SOC[14]	5.355	5.357	--	--	--	1.5	+50
	SIC-LSD[19]	5.420		209		0.8		--
	Expt[12c, 24]	5.376		205		1.3		<0
CmO_2	PBE[13]	5.456	5.439	154	155	0	0	-85
	AM05/PBE-Sol [15]	5.347		218		2.50		--
	HSE-gaussian[13]	5.460	5.398	120	174	0	0.37	17
	SIC-LSD[19]	5.37		212		0.4		--

	Expt[24b, 25]	5.357		218		--		--
BkO_2	PBE[13]	5.412	5.398	187	185	1.13	0.19	87
	HSE-gaussian[13]	5.351	5.347	226	226	3.10	2.46	17
	SIC-LSD[19]	5.36		221		1.0		--
	Expt[26]	5.334		--		--		--
CfO_2	HSE-gaussian[13]	5.313	5.311	225	225	1.30	1.95	-6
	SIC-LSD[19]	5.36		210		0.6		
	Expt[27]	5.310		--		--		>0
EsO_2	HSE-gaussian[13]	5.309	5.308	208	206	0.68	1.08	-3

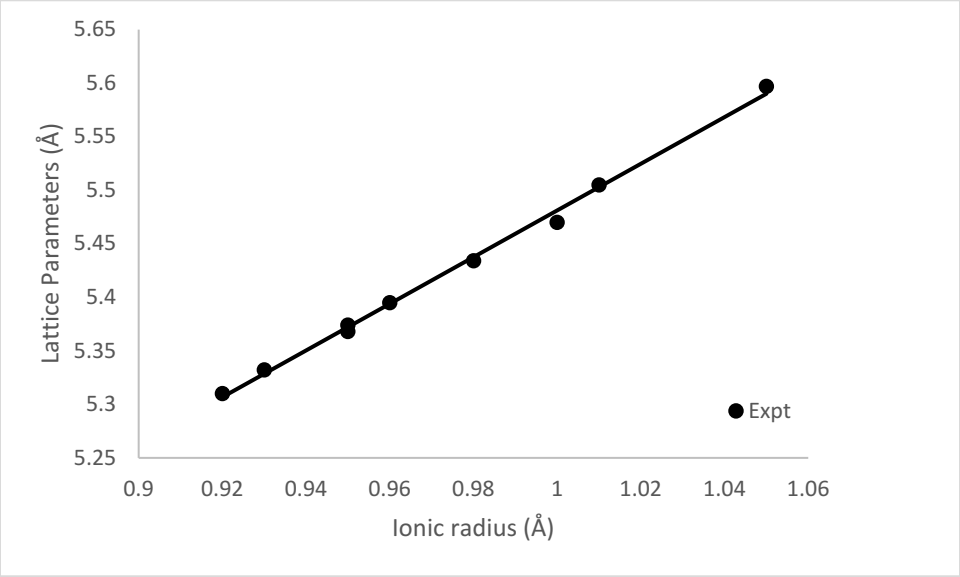

Figure 2. Experimental lattice constants as a function of ionic radii for AnO_2.

The insulating behavior is categorized based on the origin of their gap. The early actinides are associated with $f \rightarrow f$ transitions and considered Mott insulators. [28] Traversing across the series the insulating behavior changes to a O $2p \rightarrow$ An $5f$ transition, or a charge-transfer insulator.[29] The question about the magnetic ground state is also interesting and can be understood from crystal field (CF) theory (Figure 3). In the strictest formalism, spin-orbit coupling splits the *f*-shell of the cation into two sublevels, j = 7/2 and 5/2, respectively. Since the actinide cations are in a cubic environment, these levels are further split due to the crystal field. The energy level of the $|j=5/2, \Gamma_8\rangle$ quartet should be lower in energy than the $|j=5/2, \Gamma_7\rangle$ doublet due to the oxygen atoms located in the [1 1 1] direction of the actinide cations. When using this scheme, electron filling of Th^{4+} (f^0), Pu^{4+} (f^4), and Cm^{4+} (f^6) are predicted to have no effective magnetic moment (μ_B = 0) whereas U^{4+} (f^2), Np^{4+} (f^3), Am^{4+} (f^5) should have an effective moment. Although this formalism is not strictly correct, it provides a basis for predicting the bulk properties of the dioxides.

UO_2 undergoes a phase transition at T = 30.8 K, which is associated with a transverse 3***q*** antiferromagnetic structure.[30] Recent DFT+*U* calculations have confirmed the stability of the 3***q*** dipolar magnetic state.[31]

PuO_2 has a 'nonmagnetic' Γ_1 ground state which has been confirmed by Pu-NMR and exhibits temperature-independent paramagnetism up to 1000 K.[32] NpO_2 is one of the more interesting dioxides in that it exhibits a combination of octupolar and quadrupolar ordering, as confirmed by NMR measurements.[33] In AmO_2, a phase transition is observed at 8.5K however no magnetic moment has been observed in Mossbauer or neutron diffraction experiments, perhaps suggesting spin glass behavior. [34]

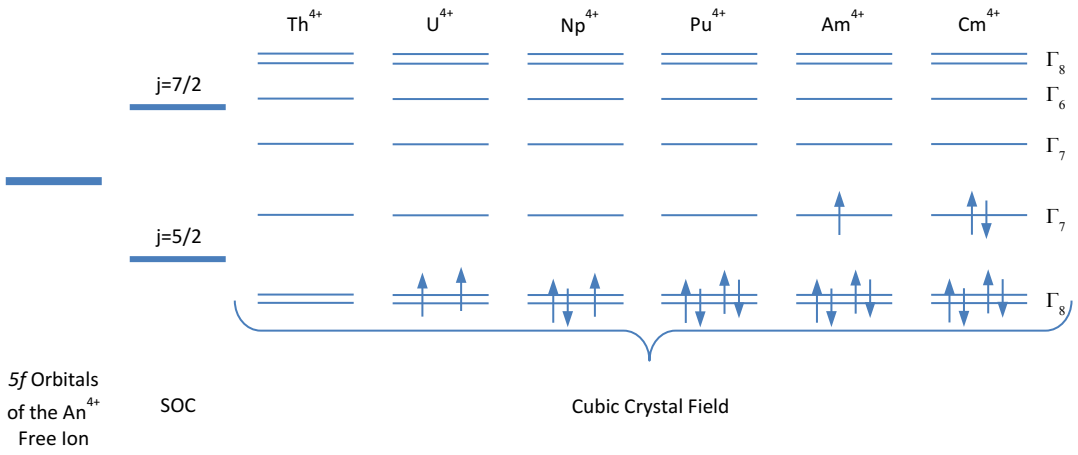

Figure 3. The f-shell splitting with spin-orbit coupling and cubic crystal field in terms of one-electron f orbitals.

The complexities seen in the dioxides including magnetic ground state, spin-orbit coupling, and crystal field effects have been highlighted in several articles and reviews, and theoretical methods have had difficulties predicting their properties.[14, 35 7a, 36] Because the functional dependencies of the dioxides are the most studied within the series, this review will provide only a high-level overview of the salient features for consistency and clarity using the lowest energy solutions from the literature. Conventional Kohn-Sham functionals in the local-density (LDA) and generalized gradient approximations (GGA) generally predict the AnO_2 series to be ferromagnetic metals with lattice parameters and cohesive parameters in generally good agreement with experiment. Optimizations using the PBE functional reproduce the lattice parameters until CmO_2 where the trend breaks down.[13] Including a Hubbard U parameter (PBE+*U*) or self-interaction correction (SIC-LSD) creates a linear correlation across the actinide series, albeit with an overestimation of the lattice constants.[14-15, 19] Of the functionals tested, the Heyd-Scuseria-Ernzerhof (HSE) screened hybrid functional approach provides the best description of the unit cell parameters over the entire series.[14] The plot in Figure 4 highlights the performance of the different methods versus experiment.

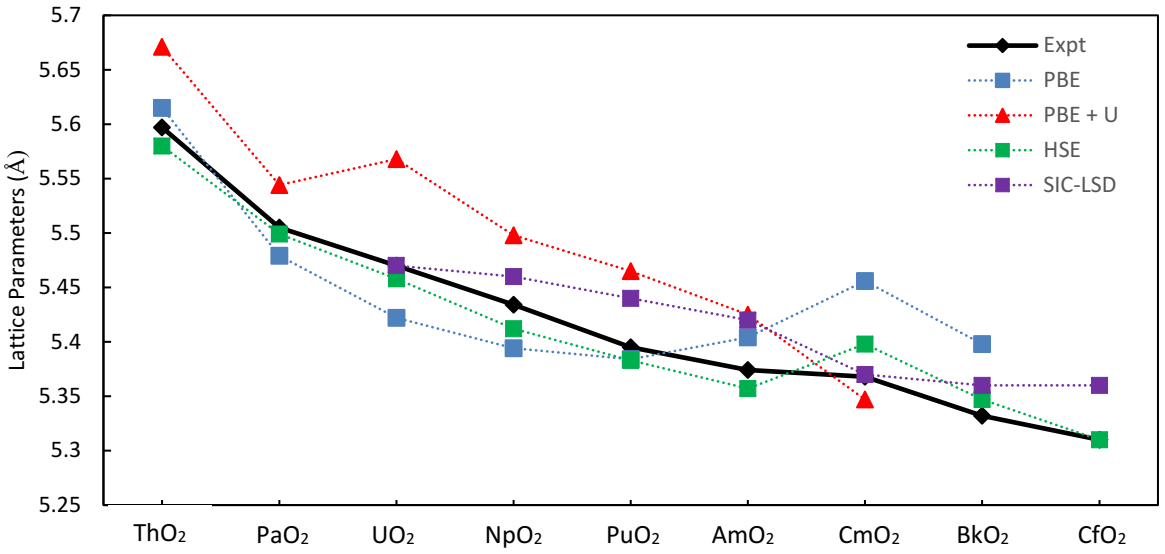

Figure 4. Lattice parameters shown in Table 1 for the AnO_2 series.

Several other properties have been reported (Table 1), including bulk modulus and band gap. The band gap problem with conventional functionals has been addressed in a number of ways to include the effects of strong correlations on the electronic structure. When adding a Hubbard U parameter, a band gap opens up that correctly predicts the Mott insulator behavior in UO_2 and the charge-transfer behavior in PuO_2.[14-15] Screened hybrid exchange-correlation functionals correctly predict the insulating behavior of the AnO_2 series, with NpO_2 predicted to be a Mott insulator.[35c] However, the band gap is also linked with long-range magnetic ordering; the oxides retain the gap in the high-temperature paramagnetic phase. There have been a few studies particularly of the light actinide dioxides using dynamical mean-field theory (DMFT) and, in combination with DFT, it has been able to predict an insulating structure without long-range ordering or local magnetic moments in PuO_2.

Figure 5 depicts the calculated band gap (eV) for several methods compared to experiment. The methods generally underpredict the band gap except in the case of the screened hybrid functional HSE. The PBE+U results are dependent upon the Hubbard U parameter used, which varies from 4 – 6 eV. Using SIC-LSD, the ground state of UO_2 is predicted to be pentavalent (f^1) and metallic; the tetravalent U^{4+} $f^2$is approximately 100 meV higher in energy with a reported band gap of 2.6 eV.[19]

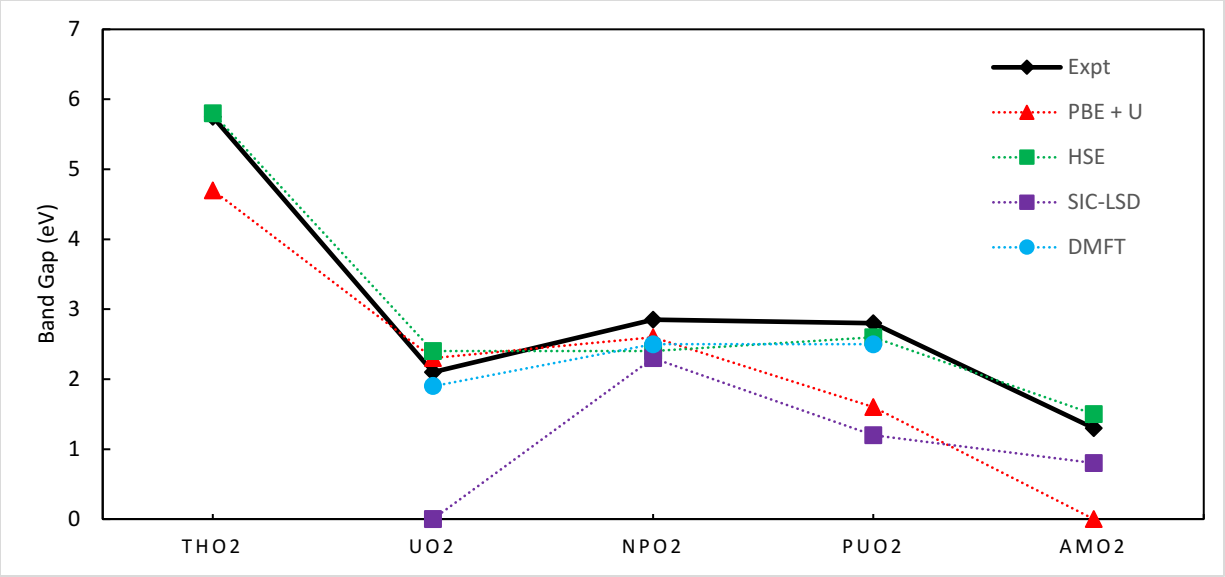

Figure 5. Band gaps (eV) shown in Table 3 for the AnO_2 series.

Covalency and orbital contributions to bonding of the actinides are of fundamental importance to understanding electronic structure and has been addressed in fuller detail in several articles and reviews.[14, 35c, 37] In summary, the actinide 5*f* and 6*d* atomic orbitals are capable of contributing to bonding with oxygen 2*p*. The general consensus for molecular systems is that upon traversing across the actinide series, the elements become more ionic, therefore less covalent interactions will occur.[38] Moffitt's seminal contribution on covalency, detailing that ligand-based orbitals could span a space of the proper symmetry to interact with either *d* or *f* orbitals, preceded a number of detailed theoretical studies.[39] In the early part of the actinide series, there is a large separation of the An 5*f* and O 2*p* states.[37b] Mixing behavior indicative of covalent interactions starts occurring with PuO_2 wherein valence band edge results in mixing of the Pu 5*f*/O 2*p* bands.[37a] A study using HSE of the AnO_2 series reveals a lattice expansion at CmO_2 compared with experiment. Prodan *et al.* attributed this behavior to the actinides having lower spin density for the latter half of the series, and suggested that the partial covalency explains their preference for the sesquioxides.[37b]

Most recent work in the dioxides has been in a systematic study within the DFT+U formalism to parametrize the most suitable Coulombic (*U*) and exchange (*j*) parameters to reproduce the experimental properties for ThO_2, UO_2, NpO_2, PuO_2, AmO_2, and CmO_2 while maintaining their respective magnetic orderings as predicted from the one electron crystal field and Russel-Saunders coupling scheme.[15] Band gap and lattice parameter performance as a function of *U* is presented in Figure 6 for the diamagnetic ordering of PuO_2. For the non-ordered AnO_2 materials (ThO_2, PuO_2, and CmO_2), excellent approximation is made for Coulomb values of U = 6.00 – 6.50 eV with newer functionals AM05 and PBE-Sol outperforming their traditional counterparts.[15] The exchange modifier (*j*) on the band gap and lattice parameters has either minor effect, or negative effect in the case of PuO_2. Hence, Pegg *et al.* concluded that higher U values with no dependency on the exchange modifier most accurately reproduces the results with AM05/PBE-Sol functionals.[15] In Figure 7, the density of states for ThO_2, PuO_2, and CmO_2 show the valence

state is comprised of O 2*p* bands with minor contributions from An 6*d* and 5*f* states. The thorium analog exhibits Mott insulator characteristics while the other two are charge-transfer insulators.

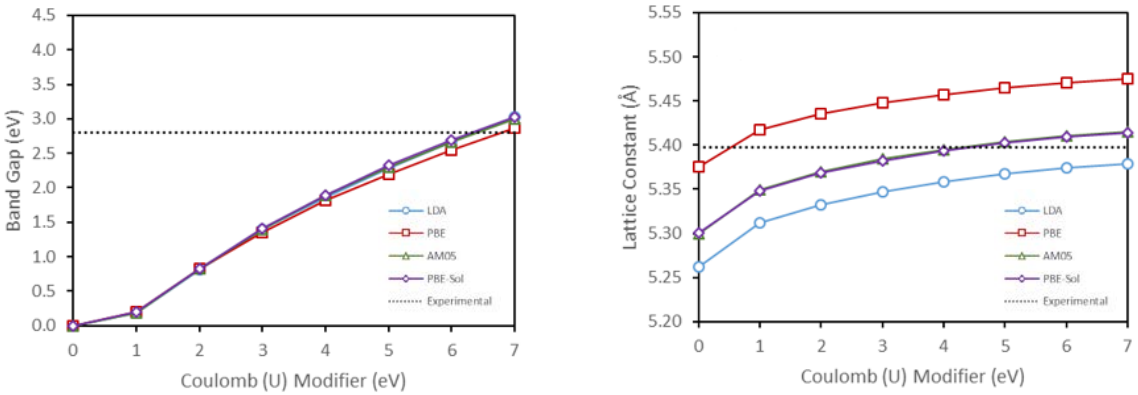

Figure 6. Band gap (left) and lattice parameter (right) dependencies as a function of U for PuO_2.[15]

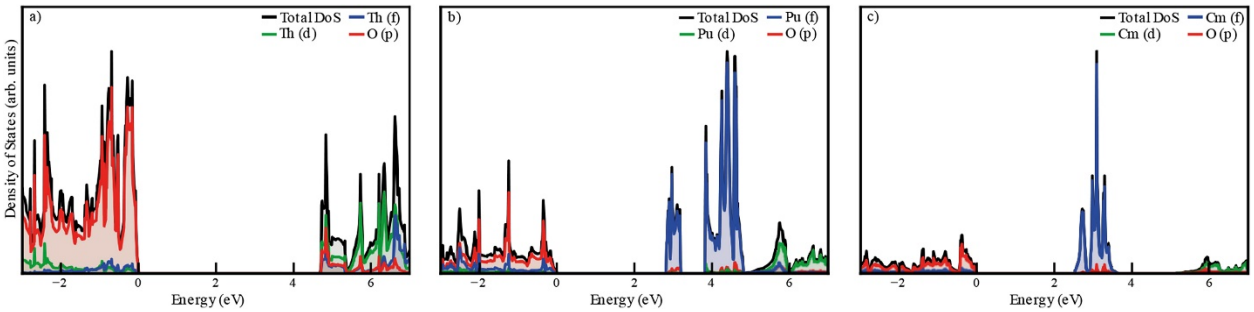

Figure 7. Calculated density of states for ThO_2(left), PuO_2(middle), and CmO_2(right) using PBE-Sol.[15]

In the ordered magnetic materials of UO_2, NpO_2, and AmO_2, the same protocol was used to benchmark the systems with Coulombic *U* and exchange *j* values ranging from 0.00 – 7.00 eV and 0.00 – 1.00 eV, respectively.[15] The calculations considered the observed magnetic ordering for UO_2 and NpO_2 (traverse and longitudinal 3***q*** AFM ordering, respectively) whereas the ordering for AmO_2 has yet to be determined. For AmO_2, a traverse 3***q*** AFM ground state was preferred based on PBE-Sol calculations. The relative band gaps, lattice parameters, and magnetic moment are shown in Figure 8 for UO_2 and, similar to the non-ordered AnO_2 materials, there is little influence on the gap based on the functional used. The biggest indicator on the choice of functional is seen in the lattice parameter, which is to be expected. Based on the reproducibility of experimental results, a lower *U* value between 3 – 4 eV is preferred for UO_2 while a higher Coulombic value between 5 and 7 eV is better for NpO_2 and AmO_2. Interestingly, an internal distortion of the oxygen ions was seen for UO_2, leading to a subtle break in symmetry to $Pa\bar{3}$.[15] When considering the exchange *j* value, calculations focused on specific properties using PBE-Sol and found that the best reproducibility for UO_2 experimental results were obtained in the absence of *j* and more dependence was seen in NpO_2 and AmO_2. Figure 9 highlights the exchange dependency on the properties for AmO_2. In contrast to the dependencies seen in the Coulombic *U* value, the exchange *j* value has influence on the band gap and magnetic moment of the Am^{4+} ion. Also, the higher *j* value leads to a much

greater internal distortion of the oxygen atoms and a break in the crystal symmetry to $Pa\bar{3}$.[15] The density of states is shown in Figure 10 and PBE-Sol with optimized *U* and *j* values correctly reproduces the expected Mott insulating behavior for UO_2 and charge-transfer behavior for NpO_2 and AmO_2.

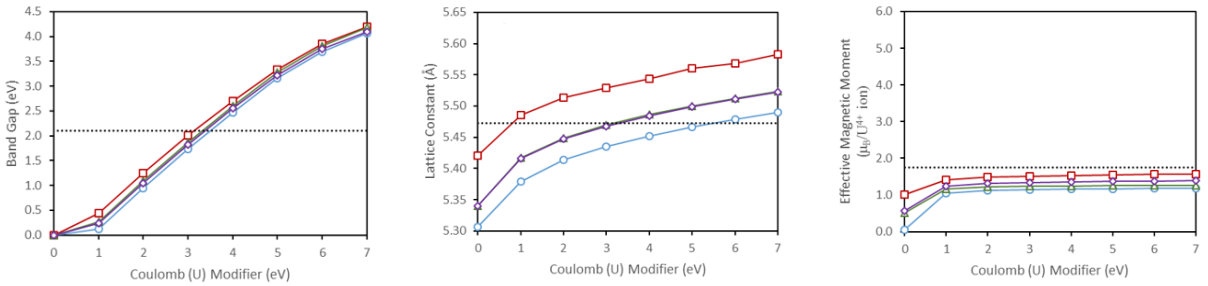

Figure 8. Calculated band gap (left), lattice parameter (middle) and effective magnetic moment (right) as a function of U for UO_2. See Figure 6 for labeling. [15]

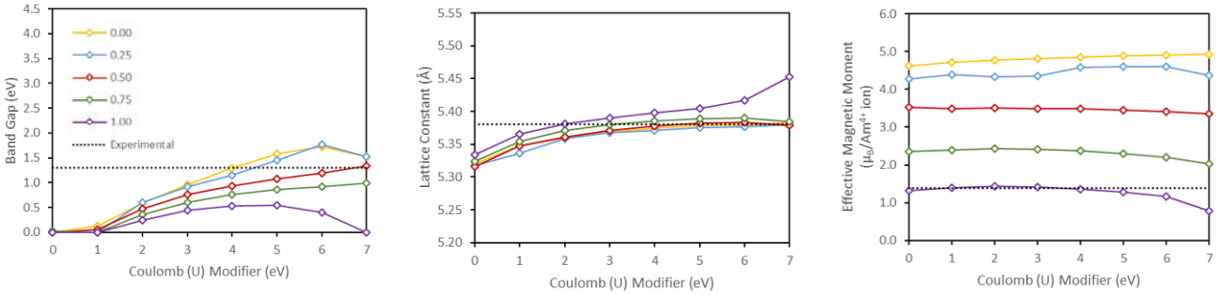

Figure 9. Calculated band gap (left), lattice parameter (middle) and effective magnetic moment (right) as a function of j for AmO_2.[15]

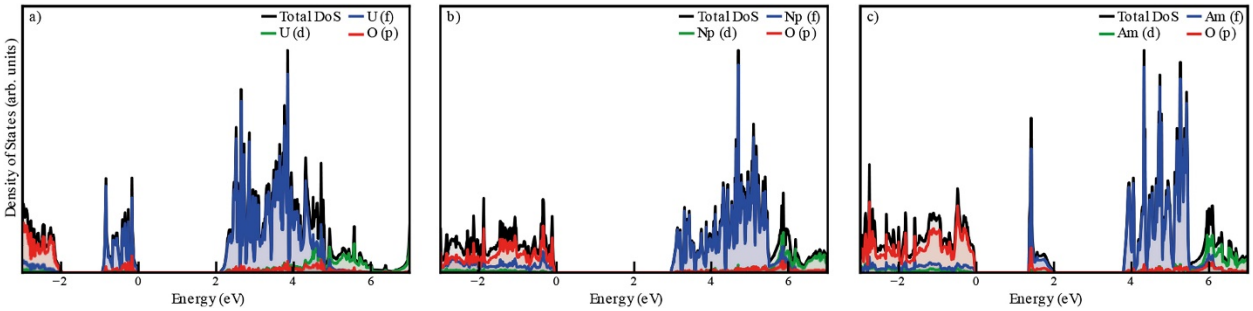

Figure 10. Calculated density of states for UO_2(left), NpO_2(middle), and AmO_2(right) using PBE-Sol.[15]

Given the high computational cost of using HSE, calculations using AM05 and PBE-Sol allows for a more attractive alternative to achieving accurate results. Table 2 lists the following *U* and *j* parameters provide accurate description of the bulk properties of the AnO_2 materials.

Table 2. Optimized Coulombic (U) and exchange (j) values in eV for AnO_2 using PBE-Sol.[15]

Compound	***U***	***J***
ThO_2	6.00	0.00
UO_2	3.35	0.00
NpO_2	5.00	0.75
PuO_2	6.35	0.00
AmO_2	7.00	0.50

CmO_2	6.00	0.00

Actinide Sesquioxide

The actinide sesquioxides are the second most common actinide oxides across the series, mainly occurring in the latter half. They can crystallize in three different polymorphs: hexagonal close-packed (A), monoclinic (B), or cubic (C).[40] The H-type and X-type polymorphic modifications found in rare earth sesquioxides have not been isolated. The hexagonal form (A-type) is stable at room temperature. The cubic structure (C-type) is closely related to the CaF_2-type structure as a 2 x 2 x 2 supercell with ¼ of the oxygen ions removed. The ideal oxidation state of the metal center is +3. Crystallographic information can be found in Table 3 with Figure 11 illustrating the structures of A-type and C-type An_2O_3.

Table 3. Crystallographic information for An_2O_3.

Phase	Cell Parameters (Å)	Symmetry	Space Group
A-Ac_2O_3[41]	a=4.08 c=6.30	Hexagonal	$P\bar{3}m1$
A-Pu_2O_3[42]	a=3.83 c=5.92	Hexagonal	$P\bar{3}m1$
C-Pu_2O_3[43]	a=11.05	Cubic	$Ia\bar{3}$
A-Am_2O_3[44]	a=3.817 c=5.971	Hexagonal	$P\bar{3}m1$
C-Am_2O_3[12a]	a=10.9	Cubic	$Ia\bar{3}$
A-Cm_2O_3[45]	a=3.799 c=5.99	Hexagonal	$P\bar{3}m1$
B-Cm_2O_3[46]	a=14.16 b=3.629 c=8.847	Monoclinic β=100.55	$C2/m$
C-Cm_2O_3[25]	a=10.996	Cubic	$Ia\bar{3}$
A-Bk_2O_3[47]	a=3.754 c=5.958	Hexagonal	$P\bar{3}m1$
B-Bk_2O_3[47]	a=14.197 b=3.606 c=8.846	Monoclinic β=100.23	$C2/m$
C-Bk_2O_3[26]	a=10.89	Cubic	$Ia\bar{3}$
A-Cf_2O_3[47]	a=3.72 c=5.96	Hexagonal	$P\bar{3}m1$
B-Cf_2O_3[27]	a=14.121 b=3.592 c=8.809	Monoclinic β=100.34	$C2/m$
C-Cf_2O_3[27]	a=10.78	Cubic	$Ia\bar{3}$
A-Es_2O_3[48]	a=3.7 c=6.0	Hexagonal	--
B-Es_2O_3[48]	a=14.1 b=3.59 c=8.80	Monoclinic β=100	--

C-Es_2O_3[48]	a=10.76	Cubic	$Ia\bar{3}$

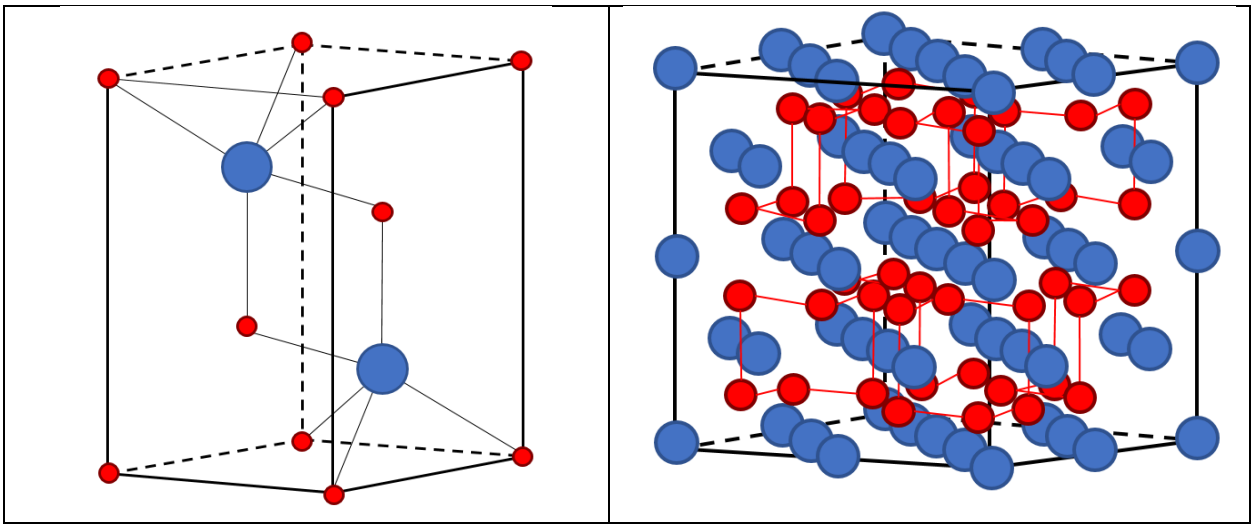

Figure 11. A-type (left) and C-type (right) An_2O_3 structures; the actinide atoms are in blue and the oxygen atoms are in red.

Theoretical studies of An_2O_3 compounds are not as prevalent in the literature as their AnO_2 counterpart, but Pu_2O_3 has been of interest given its importance in air oxidation of Pu metal.[49] Chemically, a passivated PuO_2 layer is always present on a plutonium metal surface and when exposed to dry air at room temperature, a thin layer of Pu_2O_3 found at the dioxide-metal interface. After some time, the PuO_2 layer auto-reduces to Pu_2O_3 layer. The A-type sesquioxide β-Pu_2O_3 is typically formed but the cubic form α-Pu_2O_3 has also been detected below 300 °C. With a formal Pu valence of +3 and O valence of -2, the expected electronic configuration for Pu is $5f^5$. Indeed, β-Pu_2O_3 exhibits antiferromagnetic ordering along the *z*-axis below 4.2 K.[42]

The calculated properties of β-Pu_2O_3 vs experiment are reported in Table 4. Similar to the dioxide analogue, LDA and GGA functionals predict ferromagnetic metals and post GGA treatments correctly reproduce the antiferromagnetic insulating nature of β-Pu_2O_3. The values reported in Table 4 represent the lowest energy magnetic configuration. Utilization of LDA/GGA+U approximation also leads to a band gap strongly dependent on the Coulomb interaction.[50] The SIC-LSD and DMFT methods also correctly predict insulating behavior. [19, 51] Compared to β-Pu_2O_3, less theoretical work has been done on α-Pu_2O_3 because of its structural complexity. The results are also reported in Table 4 for PBE, PBE+U (U = 4 eV), and SIC-LSD calculations.[19, 52] The ground state structure at pure PBE predicts a ferromagnetic insulator. Post GGA treatments allow the band gap to open up with a corresponding lattice expansion effect to occur.

Table 4. Calculated properties of β- and α-Pu_2O_3: equilibrium lattice constants, the bulk modulus (B), band gap for the lowest energy magnetic structure (Δ_{gap}), and magnetic energy difference ($E_{FM\text{-}AFM}$). A Coulombic parameter U = 4 eV is presented for consistency.

Phase	**Method**	**a (Å)**	**c (Å)**	**B (GPa)**	**Δ_{gap} (eV)**	**$E_{FM\text{-}AFM}$ (meV)**
β-Pu_2O_3	LSDA[50a]	3.689	5.780	181	0	-185

	PBE[50a]	3.790	5.938	146	0	-291
	LDA + U[50f]	3.849	5.573	124	1.1	18
	PBE + U[50f]	3.905	5.912	110	1.7	4
	PBE0[50a]	3.824	5.932	175	3.50	11
	HSE[13]	3.822	5.929	158	2.78	3
	EECE[50b]	3.827	6.124	120	0.82	216.3
	SIC-LSD[19]	--	--	158	2.43	--
	DMFT[51]	--	--	139	1.80	--
	Expt[42]	3.83	5.92		>0	>0
α-Pu_2O_3	PBE[52a]	10.92	--	123	0.0	<0
	PBE+U[52b]	11.20	--	128	1.7	4
	PBE+U+QA[52c]	11.222	--	127	1.90	>0
	SIC-LSD[19]	11.236	--	--	0.75	--
	Expt[53]	11.05	--	--		

For the rest of the actinide series, the electronic structures for the sesquioxides from U_2O_3 to Cf_2O_3 have been calculated for the A- and C-type structure using SIC-LSD.[19] Table 5 reports the transplutonium elements; the uranium and neptunium analogs do not exist in nature and are not included. To approximate the C-type cubic structure, a ferromagnetic spin arrangement is assumed and a simpler fluorite supercell structure was used. In addition, calculations of Am_2O_3 using PBE + U with a Hubbard U parameter of 4.8 eV are also reported.[54] For the series, the trivalent ground state configuration is preferred and are insulators with a band gap of ~2.5 eV and ~0.4 eV for the A- and C-type structures, respectively. The equilibrium volumes for the A-type structure are in good agreement with experiment, with the C-type structures overestimated by ~7%

Table 5. Calculated properties of A- and C-type An_2O_3: band gap for the lowest energy magnetic structure (Δ_{gap}), bulk modulus (B), and volume comparisons (V).

Compound	**Method**	**Δ_{gap} (eV)**	**B (GPa)**	**V_{calc} (Å^3)**	**V_{exp} (Å^3)**
A-type sesquioxides					
Am_2O_3	PBE + U[54]	2.6			
	SIC-LSD[19]	2.54	158	73.34	74.73
Cm_2O_3		3.07	168	72.40	74.53
Bk_2O_3		2.73	166	70.10	72.71
Cf_2O_3		1.78	174	69.33	71.43
C-type sesquioxides					
Am_2O_3		0.44		88.54	83.64
Cm_2O_3		0.32		86.95	83.10
Bk_2O_3		0.38		83.41	80.63
Cf_2O_3		0.47		82.60	79.59

Other Actinide Oxides

There are other oxides which have been isolated and modeled, primarily for uranium. The monoxides have been studied but not to a large extent.[19, 55] Other uranium phase crystallographic information can be found in Table 6. Since uranium exists in the U^{4+}, U^{5+}, and U^{6+} oxidations states when combined with oxygen, several intermediate oxides are formed within the range of UO_2 and UO_3 including a number of different polymorphs. Figure 12 depicts the categories based on oxide structure; oxides from UO_2 to γ-U_2O_5 have the fluorite-based, densely packed structure and δ-U_2O_5 to UO_3 are layered-type oxides with more open structures and resulting lower densities.

Table 6. Crystallographic information for uranium oxides.

Compound	Cell Parameters (Å)	Symmetry	Space Group
α-U_4O_9 [56]	a=18.93	Rhombohedral α=109.686	*R3c*
β-U_4O_9 [57]	a=21.76	Cubic	*I$\bar{4}$3d*
α-U_3O_7 [58]	a=5.46 c=5.40	Tetragonal	*I4/m*
β-U_3O_7 [57]	a=21.59 c=22.23	Tetragonal	*I$\bar{4}$2d*
γ-U_3O_7 [59]	a=5.407 c=5.597	Tetragonal	--
δ-U_3O_7 [60]	A=5.38 B=5.56 C=5.49	Monoclinic β=90.29	--
Np_2O_5 [61]	a=8.17 b=6.58 c=9.31	Monoclinic β=116.09	*P2c*
β-U_2O_5 [59]	a=3.813 c=13.180	Hexagonal	--
γ-U_2O_5 [59]	a=5.410 b=5.481 c=5.410	Monoclinic β=90.49	--
δ-U_2O_5 [59]	a=6.85 b=8.27 c=31.71	Orthorhombic	*Pnma*
α-U_3O_8 [57]	a=4.15 b=11.97 c=6.72	Orthorhombic	*Amm2*
α-U_3O_8 [62]	a=6.70 b=11.95 c=4.14	Orthorhombic	*C222*
β-U_3O_8 [63]	a=7.07 b=11.45 c=8.30	Orthorhombic	*Cmcm*
β-U_3O_8 [63]	a=11.93 b=6.72	Monoclinic	*$P2_1/m$*

	c=8.29		
γ-U_3O_8[64]	a=6.82 b=6.82 c=4.15	Orthorhombic	$P\bar{6}2m$
α-UO_3[65]	a=3.97 b=3.97 c=4.17	Trigonal	$P\bar{3}m1$
α-UO_3[66]	a=3.91 b=6.94 c=4.17	Orthorhombic	*C2mm*
β-UO_3[67]	a=10.34 b=14.33 c=3.91	Monoclinic β=99.0	$P2_1$
γ-UO_3[68]	a=6.90 c=19.98	Tetragonal	$I4_1$
γ-UO_3 [68]	a=9.79 b=19.93 c=9.71	Orthorhombic	*Fddd*
δ-UO_3 [69]	a=4.17	Cubic	$Pm\bar{3}m$
η-UO_3 [70]	a=7.51 b=5.47 c=5.22	Orthorhombic	$P2_12_12_1$

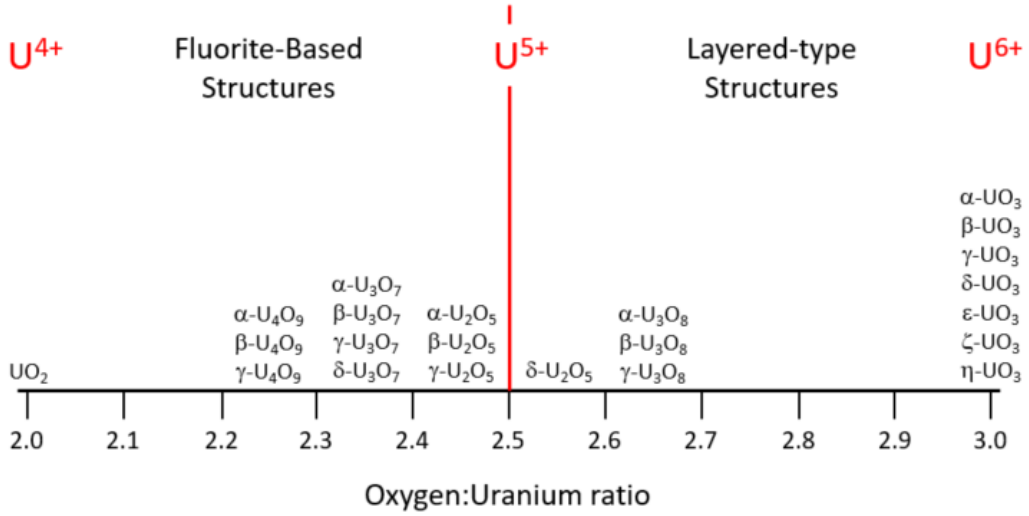

Figure 12. Illustration of the uranium oxide phases with respect to their uranium-oxygen ratio.

U_4O_9 is the first intermediate product of UO_2 oxidation and crystallizes in two closely related polymorphs which are structurally similar to UO_2. The best description for the structure is a 4 x 4 x 4 UO_2 supercell containing periodic arrangements of O_i defect clusters. There has been some debate with regards to the clustering, but the thought is that it contains a 3:1 ratio of oxygen-containing cuboctahedral clusters (COT-12) and an oxygen ion at the center of a cuboctahedral cluster (COT-13).[57] Andersson *et al.* used LSDA+U

to predict the most stable configuration contains split interstitial clusters, or two triangular di-interstitial oxygen clusters with He *et al.* predicted a band gap of 1.68 eV.[71] [72] [73] Additional work by Brincat *et al.* report stable configurations of edge-sharing 2:2:2 Willis cluster chains with PBE+U, shown in Figure 13, band gaps ranging from 1.48 to 1.61 eV.[74] As expected, the U(V) oxidation state compensates for the oxygen defects, supporting the notion that U(VI) is not a stable oxidation state for U_4O_9.

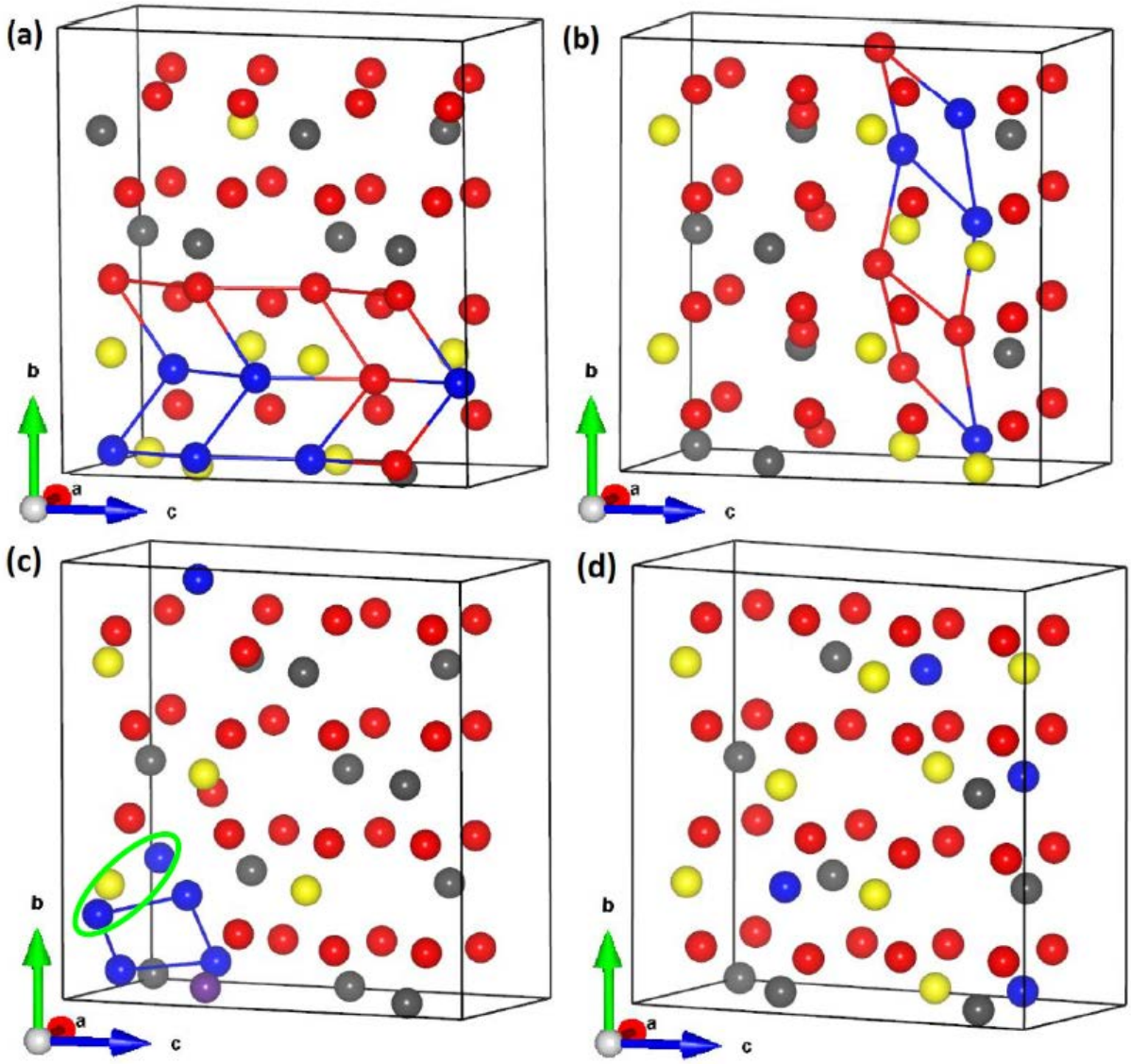

Figure 13. Relaxed U4O9 phases (a) a double 2:2:2 Willis cluster chain, (b) a single 2:2:2 Willis cluster chain, (c) a distorted 2:2:2 Willis cluster chain, and (d) four isolated O_i.[74]

U_3O_7 is a fluorite-based oxide which exhibits four non-stoichiometric polymorphs in the O/U ratio range of 2.27 to 2.38. Crystallographic information is available for α- and β- phases which have O/U ratios of 2.27 – 2.33 and 2.33 respectively. The β- phase is similar to U_4O_9 but with more nine- and then-fold coordination sites and with increased distortion to the uranium sublattice. The γ- and δ- phases are harder to isolate and only lattice parameters have been obtained. Simulations on U_3O_7 have been explored using

a 3 x 1 x1 expansion and reorientation of the UO_2 unit cell. [75] [73] The relaxed structure is a combination of U^{4+} and U^{5+} with a calculated band gap of 1.59 eV.

U_2O_5 is one of the least characterized of the uranium oxide family and represents a transition point between the known fluorite and layered structures of the series. Given the limited experimental studies, computational investigations of the structural and electronic properties provide an alternative means of characterizing U_2O_5 within the series. The α-U_2O_5 polymorph is thought to be similar to the fluorite UO_2 structure but little structural information is known. The lattice parameters for β- and γ-U_2O_5 polymorphs are known but not enough information is given on atomic positions. Complete structural information is known for δ-U_2O_5 with the uranium ions having both a pentagonal bipyramidal coordination and octahedral coordination environments (Figure 14).[59] There is some debate regarding the proper charge configuration; early XPS studies suggested a mixture of U^{4+} and U^{6+} and more recent studies have suggested U^{5+} configuration.[76] Similarly, there is also debate in the theoretical community regarding the stability of δ-U_2O_5. Brincat *et al.* showed the PBE+U was able to reproduce the structure whereas Andersson *et al.* reported the structure to be thermodynamically unstable.[73, 77]

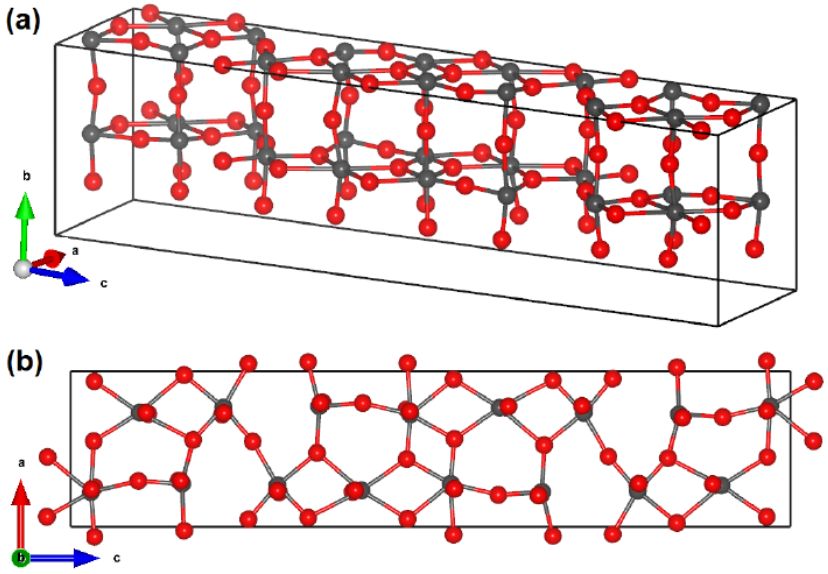

Figure 14. Structure of δ-U_2O_5. [59]

To better understand the stability, Molinari *et al.* used a novel method to identify potential phases of M_2O_5 structure types by simulating U-contained Np_2O_5, Nb_2O_5, Ta_2O_5, and V_2O_5. [78] Table 7 outlines the predicted properties of the potential U_2O_5 polymorphs and Figure 15 shows the stability plot of formation energy per U_2O_5 polymorph in eV vs. volume per U_2O_5. Molinari *et al.* determined a dependence between the formation energy and volume, with the most stable phases being Np_2O_5 followed by δ-U_2O_5.[78] The other phases follow the order of stability of Np > Nb/Ta > V. The structure for Np_2O_5 closely resembles an oxygen-deficient U_3O_8 and U^{5+} ions in both the pentagonal bipyramidal and octahedral coordination sites in the structure. Further calculations including the vibrational contribution to the free energy predicted that the Np_2O_5 phase will be thermodynamically favored over δ-U_2O_5, with the latter only stable at high

temperatures and/or pressures. The electronic properties predict all structures in Table 7 to be charge transfer insulators, with a U 5*f* conduction band and O 2*p* - U 5*f* valence band.

Table 7. Predicted properties of U_2O_5: equilibrium lattice constants, the bulk modulus (B), volume comparisons (V), band gap for the lowest energy magnetic structure (Δ_{gap}).[78]

Compound	Method	Space Group	a (Å)	b (Å)	c (Å)	β (°)	B (GPa)	V (Å^3/U_2O_5)	Δ_{gap} (eV)
δ-U_2O_5	PBE + U	*Pnma*	7.02	8.42	31.46	90	160	116.29	1.69
	Expt[59]	*Pnma*	6.85	8.27	31.71	90	--	112.27	--
Np_2O_5	PBE+U	*P2/c*	8.16	6.82	9.41	116.0	133	117.41	2.45
	Expt	*I2/a*	8.17	6.58	9.31	116.1	--	112.46	--
R-Nb_2O_5	PBE+U	*Pm*	4.21	4.35	14.98	a=106.82	149	131.63	2.07
Z-Nb_2O_5	PBE+U	*P1*	7.01	5.22	5.81	104.67	88	108.40	2.20
N-Nb_2O_5	PBE+U	*P1*	31.47	4.30	19.17	124.94	108	132.91	1.30
B-Ta_2O_5	PBE+U	$P\bar{1}$	14.29	5.30	6.14	104.40	57	112.60	2.25
α-V_2O_5	PBE+U	$P2_1$	11.54	4.36	10.60	90	82	133.45	1.99
β-V_2O_5	PBE+U	*Pm*	6.61	4.02	7.32	79.71	176	95.87	1.35

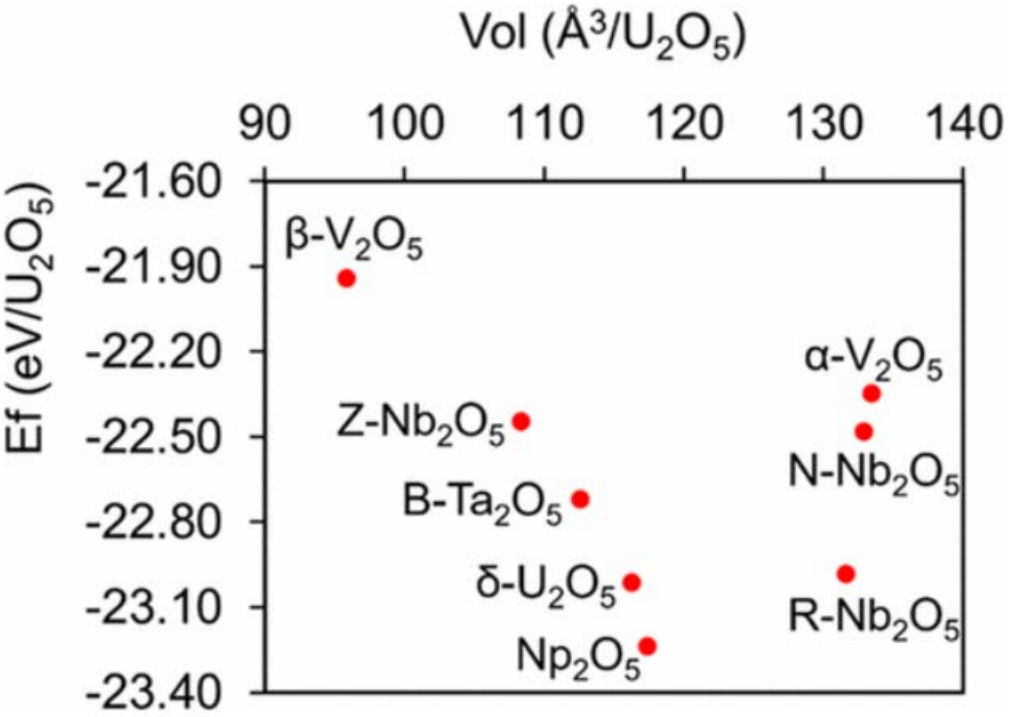

Figure 15. Plot of formation energy vs. volume for potential U_2O_5 phases.[78]

Moving away from uranium oxides discussion, the work by Molinari *et al.* highlights that neptunium also forms two oxide complexes, e.g. NpO_2 and Np_2O_5, and it is important to highlight the work that has been performed. With detailed structural information and magnetic order available, there has been some theoretical work discussing the structure, bonding, and properties of Np_2O_5.[61, 79] Np_2O_5 crystallizes in

monoclinic space group and exhibits antiferromagnetic ordering below 22 K. Yun *et al.* published several details on calculations involving Np_2O_5 in which additional Coulomb correlations on the actinide atoms are considered. Calculations predict Np_2O_5 to be an insulator with a complicated noncollinear magnetic structure (Figure 16); ferromagnetic coupling along the *c* axis with weak antiferromagnetic coupling within the *a*-*b* plane.[79] One of the Np sites has a strongly reduced moment, indicative of spin frustration of the magnetic structure. The calculated magnetic moments are sensitive to the Hubbard U parameter. The band gap as a function of U varies from 1.8 to 2.7 eV. For optimal Coulomb U of 3.5 eV, the band gap is ~ 2 eV and the 5*f* electron density spans the O 2*p* density in the valence band compared with NpO_2, implying enhanced Np 5*f*/O 2*p* hybridization for Np_2O_5. There is strong oxygen bonding present for the Np ions, causing an amount of delocalization of the 5*f* electrons. In addition, the conduction band is Np 5*f* with significant widening of the unoccupied states.

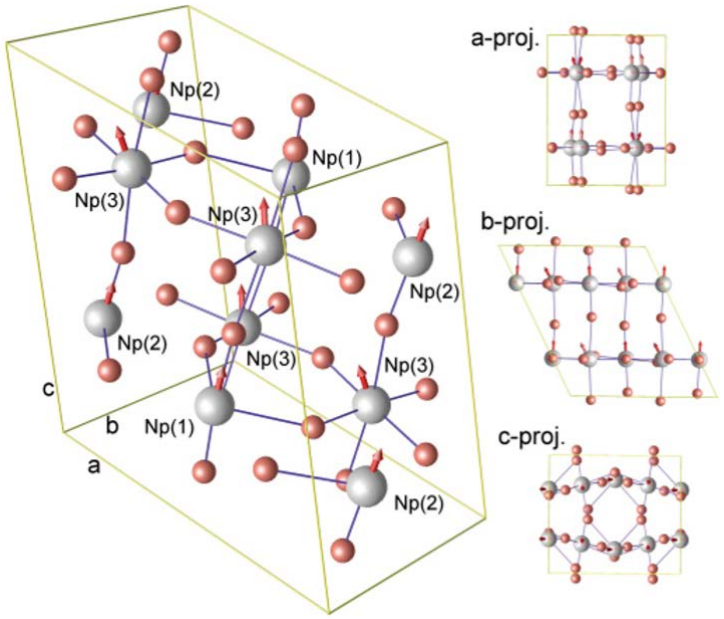

Figure 16. Noncollinear magnetic structure of Np_2O_5.[79]

Continuing on with uranium, the significance of U_3O_8 in the nuclear fuel cycle has led to a number of experimental and theoretical investigations of the structural, thermodynamic, and electronic properties of the structure. There are five U_3O_8 polymorphs and the stoichiometry suggests mixed valency with a charge configuration of one U^{4+} or two U^{6+}, or two U^{5+} and one U^{6+}. Therefore, several theoretical studies were focused on pinpointing the oxidation state with respect to structure (Table 8) with the most thorough investigation of the polymorphs was performed by Brincat *et al.*[77] The most common polymorph, α-U_3O_8, is best described as an oxygen-deficient version α-UO_3. It has been reportedly crystallized in two different orthorhombic space groups, *Amm2* and *C222*, with the uranium ions having a pentagonal bipyramidal coordination environment except for the latter structure wherein one of the two uranium sites has octahedral coordination (Figure 17).[57, 62] The predicted lowest structures of the two polymorphs from PBE+U calculations is the *C222* structure which relaxed to higher symmetry *Cmmm* upon minimization and a U^{5+}/U^{6+} charge configuration.[77] The U^{5+} ions are found at the pentagonal bipyramidal

sites whereas the U^{6+} ions reside at the octahedral sites. Comparison with the *Amm2* structure, a delocalized uranium 5.33+ charge was preferred for each site and imaginary frequencies were found, indicative of structural instability. When the charge configuration was set at U^{5+}/U^{6+}, a structural distortion was found which resembled the *C222* structure, further suggesting that the *Cmmm* modification is the preferential structure. Other theoretical work focused on the Amm2 polymorph and did not report the structural changes observed by Brincat *et al.* where the U^{4+}/U^{6+} change configuration was preferred.[73]

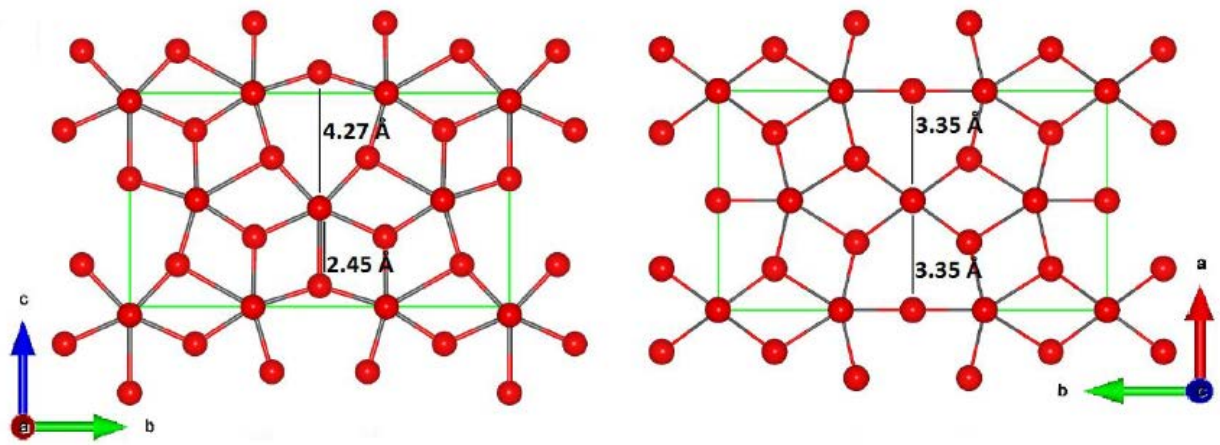

Figure 17. The experimentally observed structures for α-U_3O_8: Left – Amm2; Right – C222.

The structures β-U_3O_8 and γ-U_3O_8 are the high temperature and high pressure polymorphs, respectively, produced from α-U_3O_8. There are two polymorph for β-U_3O_8, *Cmcm* and *$P2_1/m$*, with *Cmcm* space group containing three uranium sites; two with pentagonal bipyramidal coordination and the third with octahedral coordination, similar to the *C222* polymorph of α-U_3O_8. Calculations of the two different modifications for β-U_3O_8 using PBE+U show that the *Cmcm* structure is the most energetically stable with only a slight expansion of the lattice parameters.[77] The *$P2_1/m$* polymorph relaxes to lower *P1* group with significant structural changes. For γ-U_3O_8, the structure crystallizes in *$P\bar{6}2m$* and there is a single uranium site with pentagonal bipyramidal coordination. The relaxed structure resembles the other polymorphs wherein the oxygen sublattice relaxes to allow for octahedral U^{6+} and pentagonal bypyramidal U^{5+} sites with a change in symmetry to *Amm2* upon minimization (Figure ??).

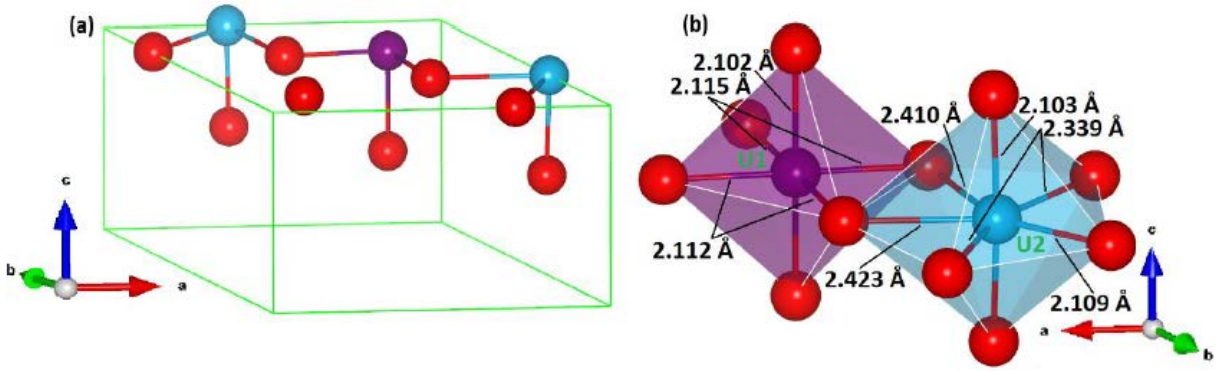

Figure 18. The optimized structure of γ-U_3O_8: Left - $P\bar{6}2m$ unit cell; Right – Uranium coordination at the two uranium sites.[77]

The predicted bulk moduli and band gaps for U_3O_8 can be also found in Table 8. While no experimental data exists, the moduli are fairly consistent except for a PBE+U calculation of α-U_3O_8 where the higher volume structure has the lowest bulk modulus.[77] The experimental band gap for α-U_3O_8 was determined using spectroscopic ellipsometry and has aided for comparison with theoretical values.[72] The PBE+U calculations overestimate the band gap by ~0.25 eV, but are still closer to other simulations in the literature where there is a large disparity among the values. This could be due, in part, to the predicted charge configuration of the uranium atoms for the various methods.

Table 8. Calculated properties of U_3O_8: Equilibrium lattice constants, the bulk modulus (B), volume comparisons (V), band gap for the lowest energy magnetic structure (Δ_{gap}). [72, 77 79-80 81]

Compound	Space Group	Method	a (Å)	b (Å)	c (Å)	B (GPa)	Vol/U (Å^3)	Δ_{gap} (eV)
α-U_3O_8	*Amm2*	LDA+U	--	--	--	--	53.91	2.43
		PBE	4.16	11.57	7.03	156.8	56.39	2.20
			4.16	11.84	6.84	168.1	56.12	1.37
		PBE+U	4.21	11.60	7.22	--	58.68	1.20
			4.24	13.06	6.60	92.5	60.92	0.71
			4.21	11.60	7.22	165.8	58.72	2.05
		PW91+U	4.21	11.61	7.20	--	58.65	0.63
		HSE	4.09	11.86	6.64	--	53.68	0.80
		Expt	4.15	11.97	6.72	--	55.55	1.76
	C222 (Cmmm)	PBE+U	7.22	11.59	4.20	169.4	58.67	2.01
		Exp	6.70	11.95	4.14		55.30	
β-U_3O_8	*Cmcm*	PBE+U	7.21	11.64	8.45	140.6	59.06	2.23
		Expt	7.07	11.45	8.30	--	55.98	
		PBE+U	11.60	7.04	8.34	132.5	56.76	1.20
			12.28	6.85	8.45	136.8	59.20	2.12
	$P2_1/m$	HSE	12.04	6.60	8.19	--	54.23	1.60
		Expt	11.93	6.72	8.29	--	55.38	--
γ-U_3O_8		PBE+U	6.84	6.84	4.17	132.5	56.31	0.0
			7.03	7.03	4.20	154.9	59.86	0.84
			6.83	6.83	4.20	181.4	56.60	2.19
		HSE	6.73	6.73	4.09	--	53.52	0.0
		Expt	6.82	6.82	4.15	--	55.76	--

UO_3 marks the endpoint for the U-O systems and has more modifications than any of the other oxides. There are seven known crystalline forms of UO_3 (α-, β-, γ-, δ-, ε- ζ-, η-) with one amorphous phase. Because of its U^{6+} ($5f^0$ electronic configuration) oxidation state, there are a variety of coordination environments with some exhibiting uranyl-like behavior, i.e. shorter axial bonds similar to the UO_2^{2+} ion (β-, γ- and η-UO_3 modifications). The α- and γ- polymorphs have been studied crystallographically, with the latter being the most thermodynamically stable with well-defined experimental data. The structures of the β, δ, η, and ε modifications are less established with ζ- being a high-pressure modification. The

most complete work on α-, β-, γ-, δ- and η-UO_3 polymorphs has been performed by Brincat *et al.* and those results, in addition to others in the literature, are reported in Table 9.[72, 81-82]

Table 9. Calculated properties of UO_3: equilibrium lattice constants, the bulk modulus (B), volume comparisons (V), band gap for the lowest energy structure (Δ_{gap}). [72, 81-83]

Compound	Space Group	Method	a (Å)	b (Å)	c (Å)	b	B (GPa)	V (Å^3)/U	Δ_{gap} (eV)
α-UO_3	*P$\bar{3}$m1*	LDA	3.80	3.80	4.14			--	
		LDA+U	--	--	--		--	53.91	0.94
		PBE+U	3.85	3.85	4.18		170.9	53.64	1.59
		HSE	--	--	--		--	59.33	3.10
		Expt	3.97	3.97	4.17		--	56.92	2.63
	C2mm	PBE+U	3.96	6.81	4.18			56.31	0.64
	C2	PBE+U	3.89	6.61	4.18		164.5	53.69	1.54
		Expt	3.91	6.94	4.17			56.55	
β-UO_3	*$P2_1$*	PBE+U	10.81	14.33	4.19	90.8	72.0	64.95	2.11
		Expt	10.34	14.33	3.91	99.0	--	57.22	2.17
γ-UO_3	*$I4_1$*	LDA+U	--	--	--			57.72	2.35
		PBE+U	7.02	7.02	20.68		74.8	63.82	2.40
		Expt	6.90	6.90	19.98			59.46	2.38
	Fddd	PBE+U	9.94	20.68	9.93		74.9	63.79	2.39
		PBE-SOL	9.71	19.72	9.75			58.35	
		Expt	9.79	19.93	9.71		--	59.16	2.38
δ-UO_3	*Pm$\bar{3}$m*	LDA	4.15	4.15	4.15		--	--	
		PBE	4.16	4.16	4.16		147.2	72.41	1.60
		LDA+U	--	--	--		--	71.21	2.19
		PBE+U	4.20	4.20	4.20		151.3	73.89	2.19
		HSE	--	--	--		--	69.27	3.21
		Expt	4.17	4.17	4.17		--	72.25	2.17
η-UO_3	*$P2_12_12_1$*	LDA	7.51	5.52	5.27		--	--	--
		PBE+U	7.76	5.56	5.34		89.2	57.60	2.67
		Expt	7.51	5.47	5.22		-	53.62	--

α-UO_3 is structurally similar to α-U_3O_8 and has been crystallized as 2 different polymorphs in the hexagonal *P$\bar{3}$m1* and orthorhombic *C2mm* space groups (Figure 19). To determine the lowest energy structure, Brincat *et al.* calculated the structural properties using PBE + U for the two modifications and found the *P$\bar{3}$m1* structure to be the most energetically stable, maintaining the same space group and coordination environment.[82] The *C2mm* structure exhibited a distortion of the coordination environment upon optimization, which forced the symmetry to *C2* and resemble more of the *P$\bar{3}$m1* structure. Some additional DFT studies have been done using LDA+U and HSE functionals on the experimental structure and the band gap is similar.[72, 81] The largest structural difference that can occur between experimental and optimized DFT calculations appear in β-UO_3 where the relaxed structure exhibits more lattice parameter and bond changes compared to the other polymorphs in the series.[82] γ-UO_3 is the most stable

UO_3 polymorph and has been crystallized in 2 different modifications, orthorhombic *Fddd* and tetragonal $I4_1$ structures. Loopstra later used neutron diffraction over a range of temperatures identifying the Fddd structure below 293K and tetragonal $I4_1$ above 373 K.[68] The structures are very similar with the orthorhombic cell double the size of the tetragonal cell with both containing two uranium sites and three oxygen sites. The minimized structures are similar with predicted volumes and relaxed bond lengths nearly identical; the *Fddd* structure is a 45° rotation and $\sqrt{2}$ expansion of the $I4_1$ polymorph in the *x* and *y* directions.[82] The δ-phase crystallizes in the $Pm\bar{3}m$ space group and with U atoms in a perfect octahedral environment and no uranyl-type bonds present. In the η- modification, the U atoms exhibit 7-fold puckered pentagonal bipyramidal coordination environment with uranyl-type bonding.

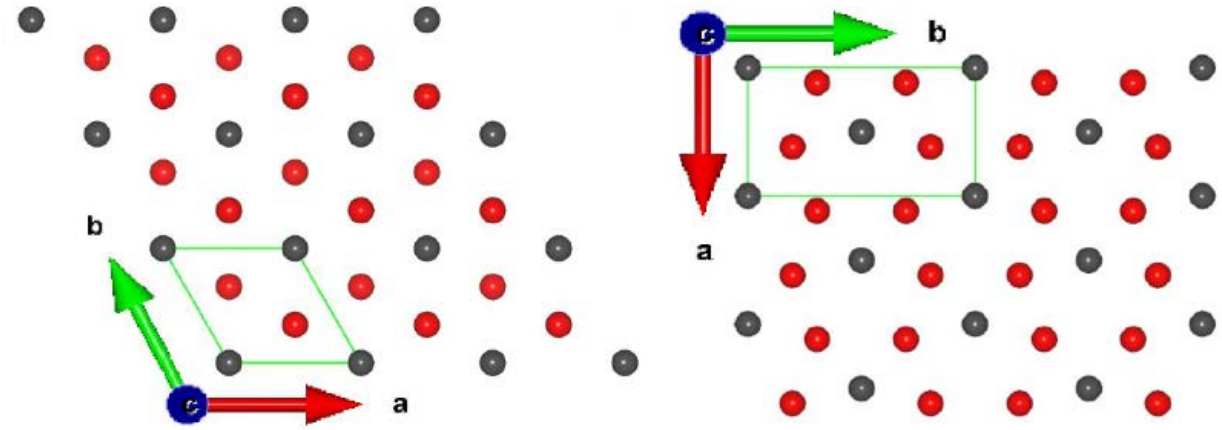

Figure 19. Structure of the $P\bar{3}m1$ (left) and C2mm (right) α-UO_3 polymorphs.

Property information is sparse for UO_3. The predicted bulk moduli range from ~70 to 170 GPa, with the higher values for α- and δ-UO_3. An interesting observation from Brincat *et al.* is an inverse relationship between the calculated bulk modulus and the density of the material.[82] Also, if the bulk modulus is less than 100 GPa, the oxide likely contains uranyl bonds (β-, γ- and η-UO_3) versus higher values where they are probably absent (α- and δ-UO_3). For the electronic properties, the U^{6+} ion has unoccupied 5*f* states and the polymorphs are charge-transfer insulators with the valance and conduction band predominantly composed of O 2*p* and U 5*f*, respectively. There is a limited amount of hybridization with contributions from 5*f* orbitals in the valence band. The calculated band gaps show that the functionals perform well for β-, γ- and δ-UO_3; the band gap prediction for α-UO_3 is more sporadic with a range of 0.64 – 3.10 eV.[82] Figure 20 shows the relative stabilities of the UO_3 polymorphs with respect to pressure based on PBE + U calculations with results standardized with respect to γ-UO_3, the thermodynamically stable phase.[82] At zero pressure, α-UO_3 is the least stable phase, similar to experiment. As the pressure increases, the stability of the η- phase is lowered to the point at which it becomes most stable and the δ-UO_3 polymorph is the least stable. The relative stability could be related to the presence of uranyl-type bonds in the structure, but no trend emerges from the calculations.[82]

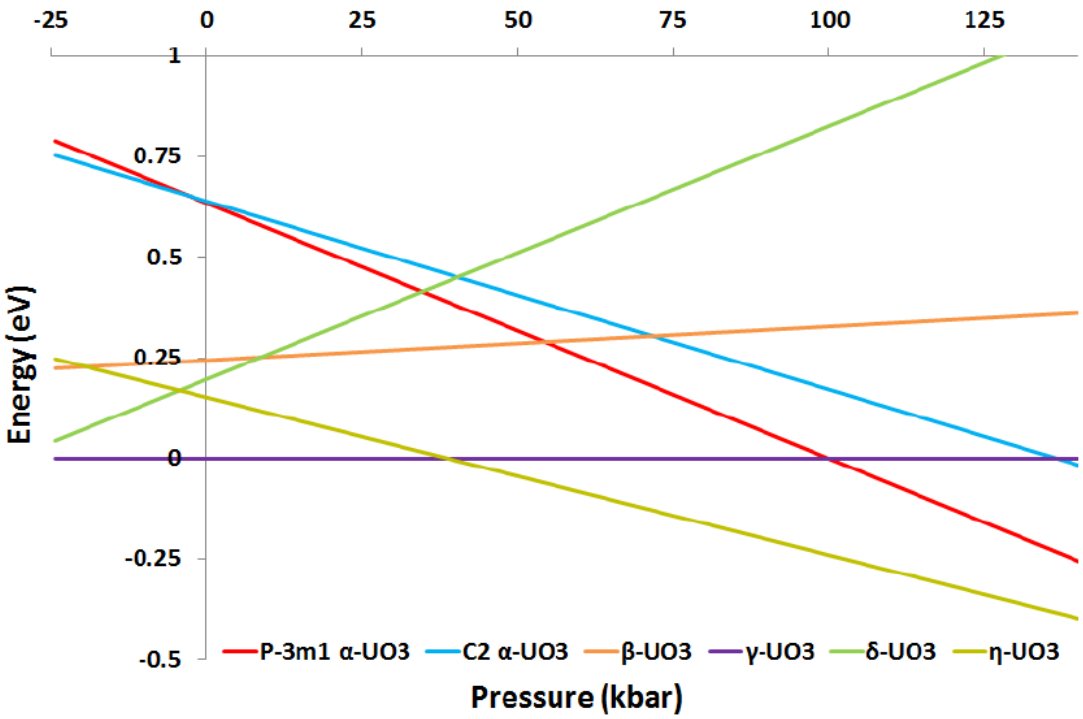

Figure 20. Calculated enthalpy of formation for UO_3 phases with PBE + U as a function of pressure.[82]

Concluding Remarks

This review has demonstrated that DFT has made considerable progress over the past 20 years in predicting the electronic structure and properties of the actinide oxides, in particular with lattice constants, densities of states, band gaps, and magnetic properties. However, more work needs to be done to accurately describe the chemical and physical properties of *f*-element structures. The development of the screened hybrid functional HSE has provided a means of predicting the properties of the actinide oxides without *a priori* knowledge of the specific parameters, but at a large computational cost. The DFT+*U* approach can predict properties, but there is still no consensus in the community regarding the optimal parameters. The recent work by Pegg *et al.* could be expanded into a systematic study of various actinide oxides for determination of accurate Coulombic (*U*) and exchange (*j*) parameters for a specific functional. In addition, the field needs to also consider development of a computational screening method for difficult phases utilizing a machine learning approach.[84] Once new phases are identified, experimentalists should attempt to verify theoretical results such as the work presented by Molinari *et al*.[78] Finally, new DFT techniques should be tested and verified by the community to resolve issues, such as the self-interaction error (SIE) that is inherent in DFT and is especially problematic for *f*-element systems. DFT+*U* has proven to be a popular choice for actinide systems given its good trade-off between accuracy and computational efficiency. The emergence of occupation matrix control, which works by controlling the orbital occupation in the DFT+*U* calculation through occupation matrices, provides an interesting tool for testing different atomic positions for localized electronic states.[85] There has been some work started in this direction.[50f, 86] While the problems remain challenging, it's clear that

the field will continue to push the bounds of theoretical methods to ultimately lead to a predictive science for development of new nuclear materials.

References

1. Eccles, H., NUCLEAR FUEL CYCLE TECHNOLOGIES -SUSTAINABLE IN THE TWENTY FIRST CENTURY? *Solvent Extraction and Ion Exchange* **2000,** *18* (4), 633-654.
2. Brown, C., Introduction: MOX fuel - electricity generation from plutonium recycling. *Nucl. Eng. (Inst. Nucl. Eng.)* **1996,** *37* (6), 166.
3. (a) Konings, R. J. M., Thermochemical and thermophysical properties of curium and its oxides. *Journal of Nuclear Materials* **2001,** *298* (3), 255-268; (b) AGENCY, I. A. E., *Advanced Reactor Technology Options for Utilization and Transmutation of Actinides in Spent Nuclear Fuel*. INTERNATIONAL ATOMIC ENERGY AGENCY: Vienna, 2009.
4. Orr, R. M.; Sims, H. E.; Taylor, R. J., A review of plutonium oxalate decomposition reactions and effects of decomposition temperature on the surface area of the plutonium dioxide product. *J. Nucl. Mater.* **2015,** *465*, 756-773.
5. Vigier, J.-F.; Freis, D.; Pöml, P.; Prieur, D.; Lajarge, P.; Gardeur, S.; Guiot, A.; Bouëxière, D.; Konings, R. J. M., Optimization of Uranium-Doped Americium Oxide Synthesis for Space Application. *Inorganic Chemistry* **2018,** *57* (8), 4317-4327.
6. (a) Ismagilov, Z. R.; Lazareva, S. V., Synthesis and Characterization of Uranium-containing Catalysts. *Catalysis Reviews* **2013,** *55* (2), 135-209; (b) Hutchings, G. J.; Heneghan, C. S.; Hudson, I. D.; Taylor, S. H., Uranium-oxide-based catalysts for the destruction of volatile chloro-organic compounds. *Nature* **1996,** *384*, 341; (c) D. Pollington, S.; F. Lee, A.; L. Overton, T.; J. Sears, P.; B. Wells, P.; E. Hawley, S.; D. Hudson, I.; F. Lee, D.; Ruddock, V., Novel supported uranium oxide catalysts for NO abatement. *Chemical Communications* **1999,** (8), 725-726; (d) Chang, C.-C., Studies of the fischer-tropsch process on uranium catalysts. *Inorganica Chimica Acta* **1984,** *94* (5), 259-262; (e) Grasselli, R. K.; Callahan, J. L., Structure-catalytic efficiency relationships in U□Sb oxide acrylonitrile synthesis catalysts. *Journal of Catalysis* **1969,** *14* (1), 93-103.
7. (a) Ramanantoanina, H.; Kuri, G.; Daul, C.; Bertsch, J., Core electron excitations in U4+: modelling of the nd105f2 → nd95f3 transitions with n = 3, 4 and 5 by ligand field tools and density functional theory. *Phys. Chem. Chem. Phys.* **2016,** *18* (28), 19020-19031; (b) Nishi, T.; Nakada, M.; Itoh, A.; Suzuki, C.; Hirata, M.; Akabori, M., EXAFS and XANES studies of americium dioxide with fluorite structure. *Journal of Nuclear Materials* **2008,** *374* (3), 339-343; (c) Nishi, T.; Nakada, M.; Suzuki, C.; Shibata, H.; Itoh, A.; Akabori, M.; Hirata, M., Local and electronic structure of Am2O3 and AmO2 with XAFS spectroscopy. *J. Nucl. Mater.* **2010,** *401* (1-3), 138-142; (d) Prieur, D.; Martin, P. M.; Jankowiak, A.; Gavilan, E.; Scheinost, A. C.; Herlet, N.; Dehaudt, P.; Blanchart, P., Local Structure and Charge Distribution in Mixed Uranium-Americium Oxides: Effects of Oxygen Potential and Am Content. *Inorg. Chem.* **2011,** *50* (24), 12437-12445.
8. Perdew, J. P.; Zunger, A., Self-interaction correction to density-functional approximations for many-electron systems. *Physical Review B* **1981,** *23* (10), 5048-5079.
9. Anisimov, V. I., *Strong coulomb correlations in electronic structure calculations : beyond the local density approximation*. Gordon and Breach Science Publishers: Amsterdam, The Netherlands, 2000.
10. Georges, A.; Kotliar, G.; Krauth, W.; Rozenberg, M. J., Dynamical mean-field theory of strongly correlated fermion systems and the limit of infinite dimensions. *Reviews of Modern Physics* **1996,** *68* (1), 13-125.
11. (a) Heyd, J.; Scuseria, G. E.; Ernzerhof, M., Hybrid functionals based on a screened Coulomb potential. *The Journal of Chemical Physics* **2003,** *118* (18), 8207-8215; (b) Heyd, J.; Scuseria, G. E.;

Ernzerhof, M., Erratum: “Hybrid functionals based on a screened Coulomb potential” [J. Chem. Phys. 118, 8207 (2003)]. *The Journal of Chemical Physics* **2006,** *124* (21), 219906.
12. (a) Chikalla, T. D.; Eyring, L., Phase relationships in the americium-oxygen system. *Journal of Inorganic and Nuclear Chemistry* **1968,** *30* (1), 133-145; (b) Fahey, J. A.; Turcotte, R. P.; Chikalla, T. D., Thermal expansion of the actinide dioxides. *Inorganic and Nuclear Chemistry Letters* **1974,** *10* (6), 459-465; (c) Idiri, M.; Le Bihan, T.; Heathman, S.; Rebizant, J., Behavior of actinide dioxides under pressure: $\mathrm{U}{\mathrm{O}}_{2}$ and $\mathrm{Th}{\mathrm{O}}_{2}$. *Physical Review B* **2004,** *70* (1), 014113; (d) Fournier, J. M.; Blaise, A.; Amoretti, G.; Caciuffo, R.; Larroque, J.; Hutchings, M. T.; Osborn, R.; Taylor, A. D., High-energy-neutron spectroscopy of crystal-field excitations in ${\mathrm{NpO}}_{2}$. *Physical Review B* **1991,** *43* (1), 1142-1145.
13. Prodan, I. D. Hybrid density functional studies of bulk actinide oxides. 2006.
14. Wen, X.-D.; Martin, R. L.; Roy, L. E.; Scuseria, G. E.; Rudin, S. P.; Batista, E. R.; McCleskey, T. M.; Scott, B. L.; Bauer, E.; Joyce, J. J.; Durakiewicz, T., Effect of spin-orbit coupling on the actinide dioxides AnO2 (An=Th, Pa, U, Np, Pu, and Am): A screened hybrid density functional study. *The Journal of Chemical Physics* **2012,** *137* (15), 154707.
15. Pegg, J. T.; Aparicio-Anglès, X.; Storr, M.; de Leeuw, N. H., DFT+U study of the structures and properties of the actinide dioxides. *Journal of Nuclear Materials* **2017,** *492*, 269-278.
16. Yamashita, T.; Nitani, N.; Tsuji, T.; Inagaki, H., Thermal expansions of NpO2 and some other actinide dioxides. *Journal of Nuclear Materials* **1997,** *245* (1), 72-78.
17. Griffiths, T. R.; Dixon, J., Electron irradiation of single crystal thorium dioxide and electron transfer reactions. *Inorganica Chimica Acta* **2000,** *300-302*, 305-313.
18. Sellers, P. A.; Fried, S.; Elson, R. E.; Zachariasen, W. H., The Preparation of Some Protactinium Compounds and the Metal1. *Journal of the American Chemical Society* **1954,** *76* (23), 5935-5938.
19. Petit, L.; Svane, A.; Szotek, Z.; Temmerman, W. M.; Stocks, G. M., Electronic structure and ionicity of actinide oxides from first principles. *Physical Review B* **2010,** *81* (4), 045108.
20. Yin, Q.; Kutepov, A.; Haule, K.; Kotliar, G.; Savrasov, S. Y.; Pickett, W. E., Electronic correlation and transport properties of nuclear fuel materials. *Physical Review B* **2011,** *84* (19), 195111.
21. Meek, T. T.; von Roedern, B.; Clem, P. G.; Hanrahan, R. J., Some optical properties of intrinsic and doped UO2 thin films. *Materials Letters* **2005,** *59* (8), 1085-1088.
22. Suzuki, C.; Nishi, T.; Nakada, M.; Akabori, M.; Hirata, M.; Kaji, Y., Core-hole effect on XANES and electronic structure of minor actinide dioxides with fluorite structure. *Journal of Physics and Chemistry of Solids* **2012,** *73* (2), 209-216.
23. McCleskey, T. M.; Bauer, E.; Jia, Q.; Burrell, A. K.; Scott, B. L.; Conradson, S. D.; Mueller, A.; Roy, L.; Wen, X.; Scuseria, G. E.; Martin, R. L., Optical band gap of NpO2 and PuO2 from optical absorbance of epitaxial films. *Journal of Applied Physics* **2013,** *113* (1), 013515.
24. (a) Asprey, L. B.; Ellinger, F. H.; Fried, S.; Zachariasen, W. H., EVIDENCE FOR QUADRIVALENT CURIUM: X-RAY DATA ON CURIUM OXIDES1. *Journal of the American Chemical Society* **1955,** *77* (6), 1707-1708; (b) Dancausse, J. P.; Haire, R. G.; Heathman, S.; Benedict, U., High-Pressure X-ray Diffraction Studies of Americium and Curium Dioxides. *Journal of Nuclear Science and Technology* **2002,** *39* (sup3), 136-139.
25. Mosley, W. C., Phases and transformations in the curium-oxygen system. *J. Inorg. Nucl. Chem.* **1972,** *34* (2), 539-55.
26. Baybarz, R. D., Berkelium oxide system. *J. Inorg. Nucl. Chem.* **1968,** *30* (7), 1769-73.
27. Baybarz, R. D.; Haire, R. G.; Fahey, J. A., On the californium oxide system. *Journal of Inorganic and Nuclear Chemistry* **1972,** *34* (2), 557-565.
28. An, Y. Q.; Taylor, A. J.; Conradson, S. D.; Trugman, S. A.; Durakiewicz, T.; Rodriguez, G., Ultrafast Hopping Dynamics of $5f$ Electrons in the Mott Insulator ${\mathrm{UO}}_{2}$ Studied by Femtosecond Pump-Probe Spectroscopy. *Physical Review Letters* **2011,** *106* (20), 207402.

29. Zaanen, J.; Sawatzky, G. A.; Allen, J. W., Band gaps and electronic structure of transition-metal compounds. *Physical Review Letters* **1985,** *55* (4), 418-421.
30. (a) Willis, B. T. M.; Taylor, R. I., Neutron diffraction study of antiferromagnetism in UO2. *Physics Letters* **1965,** *17* (3), 188-190; (b) Carretta, S.; Santini, P.; Caciuffo, R.; Amoretti, G., Quadrupolar Waves in Uranium Dioxide. *Physical Review Letters* **2010,** *105* (16), 167201; (c) Wilkins, S. B.; Caciuffo, R.; Detlefs, C.; Rebizant, J.; Colineau, E.; Wastin, F.; Lander, G. H., Direct observation of electric-quadrupolar order in $\mathrm{U}{\mathrm{O}}_{2}$. *Physical Review B* **2006,** *73* (6), 060406.
31. (a) Laskowski, R.; Madsen, G. K. H.; Blaha, P.; Schwarz, K., Magnetic structure and electric-field gradients of uranium dioxide: An ab initio study. *Physical Review B* **2004,** *69* (14), 140408; (b) Zhou, F.; Ozoliņš, V., Crystal field and magnetic structure of UO${}_{2}$. *Physical Review B* **2011,** *83* (8), 085106.
32. (a) Yasuoka, H.; Koutroulakis, G.; Chudo, H.; Richmond, S.; Veirs, D. K.; Smith, A. I.; Bauer, E. D.; Thompson, J. D.; Jarvinen, G. D.; Clark, D. L., Observation of ²³⁹Pu Nuclear Magnetic Resonance. *Science* **2012,** *336* (6083), 901-904; (b) Raphael, G.; Lallement, R., Susceptibilite magnetique de PuO2. *Solid State Communications* **1968,** *6* (6), 383-385.
33. (a) Sakai, O.; Shiina, R.; Shiba, H., Invariant Form of Multipolar Interactions and Relation between Antiferro-Quadrupolar Order and Field-Induced Magnetic Moments. *Journal of the Physical Society of Japan* **2003,** *72* (6), 1534-1543; (b) Tokunaga, Y.; Aoki, D.; Homma, Y.; Kambe, S.; Sakai, H.; Ikeda, S.; Fujimoto, T.; Walstedt, R. E.; Yasuoka, H.; Yamamoto, E.; Nakamura, A.; Shiokawa, Y., NMR Evidence for Higher-Order Multipole Order Parameters in ${\mathrm{NpO}}_{2}$. *Physical Review Letters* **2006,** *97* (25), 257601; (c) Tokunaga, Y.; Aoki, D.; Homma, Y.; Kambe, S.; Sakai, H.; Ikeda, S.; Fujimoto, T.; Walstedt, R. E.; Yasuoka, H.; Shiokawa, Y.; Yamamoto, E.; Nakamura, A., NMR observation of quadrupolar order parameter in NpO2. *Journal of Magnetism and Magnetic Materials* **2007,** *310* (2, Part 1), 735-737.
34. (a) Karraker, D. G., Magnetic susceptibility of 243AmO2 *The Journal of Chemical Physics* **1975,** *63* (7), 3174-3175; (b) Abraham, M. M.; Boatner, L. A.; Finch, C. B.; Reynolds, R. W., Electron-Paramagnetic-Resonance Investigations of $5{f}^{5}$ Configuration Ions in Cubic Single Crystals: ${\mathrm{Pu}}^{3+}$ in Th${\mathrm{O}}_{2}$ and Sr${\mathrm{Cl}}_{2}$, and ${\mathrm{Am}}^{4+}$ in Th${\mathrm{O}}_{2}$. *Physical Review B* **1971,** *3* (9), 2864-2868; (c) Kolbe, W.; Edelstein, N.; Finch, C. B.; Abraham, M. M., Electron paramagnetic resonance of 239Pu3+ and 243Am4+ in CeO2 and of 241Pu3+ in ThO2. *The Journal of Chemical Physics* **1974,** *60* (2), 607-609; (d) Hotta, T., Microscopic analysis of multipole susceptibility of actinide dioxides: A scenario of multipole ordering in ${\text{AmO}}_{2}$. *Physical Review B* **2009,** *80* (2), 024408; (e) Tokunaga, Y.; Nishi, T.; Kambe, S.; Nakada, M.; Itoh, A.; Homma, Y.; Sakai, H.; Chudo, H., NMR Evidence for the 8.5 K Phase Transition in Americium Dioxide. *Journal of the Physical Society of Japan* **2010,** *79* (5), 053705; (f) Tokunaga, Y.; Nishi, T.; Kambe, S.; Nakada, M.; Homma, Y.; Sakai, H.; Chudo, H., NMR Study on AmO2: Comparison with UO2 and NpO2. *Journal of the Physical Society of Japan* **2011,** *80* (Suppl.A), SA110.
35. (a) Boettger, J. C., Predicted spin-orbit coupling effect on the magnetic ordering of crystalline uranium dioxide. *Eur. Phys. J. B* **2003,** *36* (1), 15-20; (b) Nakamura, H.; Machida, M.; Kato, M., Effects of spin-orbit coupling and strong correlation on the paramagnetic insulating state in plutonium dioxides. *Phys. Rev. B: Condens. Matter Mater. Phys.* **2010,** *82* (15), 155131/1-155131/6; (c) Wen, X.-D.; Martin, R. L.; Henderson, T. M.; Scuseria, G. E., Density Functional Theory Studies of the Electronic Structure of Solid State Actinide Oxides. *Chemical Reviews* **2013,** *113* (2), 1063-1096.
36. (a) Suzuki, M. T.; Magnani, N.; Oppeneer, P. M., Microscopic theory of the insulating electronic ground states of the actinide dioxides AnO${}_{2}$ (An = U, Np, Pu, Am, and Cm). *Physical Review B* **2013,** *88* (19), 195146; (b) Hoover, M. E.; Atta-Fynn, R.; Ray, A. K., Surface properties of uranium dioxide from first principles. *Journal of Nuclear Materials* **2014,** *452* (1), 479-485.
37. (a) Prodan, I. D.; Scuseria, G. E.; Martin, R. L., Assessment of metageneralized gradient approximation and screened Coulomb hybrid density functionals on bulk actinide oxides. *Phys. Rev. B:*

Condens. Matter Mater. Phys. **2006,** *73* (4), 045104/1-045104/10; (b) Prodan, I. D.; Scuseria, G. E.; Martin, R. L., Covalency in the actinide dioxides: Systematic study of the electronic properties using screened hybrid density functional theory. *Phys. Rev. B: Condens. Matter Mater. Phys.* **2007,** *76* (3), 033101/1-033101/4.
38. Kaltsoyannis, N., Does Covalency Increase or Decrease across the Actinide Series? Implications for Minor Actinide Partitioning. *Inorg. Chem.* **2013,** *52* (7), 3407-3413.
39. Moffitt, W., Atoms in molecules and crystals. *Proc. R. Soc. London, Ser. A* **1951,** *210*, 245-68.
40. Gueneau, C.; Chartier, A.; Van Brutzel, L. In *Thermodynamic and thermophysical properties of the actinide oxides*, Elsevier B.V.: 2012; pp 21-59.
41. Zachariasen, W. H., Crystal-chemical studies of the 5f series of elements. XII. New compounds representing known structure types. *Acta Crystallogr.* **1949,** *2*, 388-90.
42. Wulff, M.; Lander, G. H., Magnetic structure and plutonium ground state in plutonium oxide (β-Pu2O3). *J. Chem. Phys.* **1988,** *89* (5), 3295-9.
43. Chikalla, T. D.; McNeilly, C. E.; Skavdahl, R. E., The plutonium-oxygen system. *J. Nucl. Mater.* **1964,** *12* (2), 131-41.
44. Templeton, D. H.; Dauben, C. H., Crystal structures of americium compounds. *J. Am. Chem. Soc.* **1953,** *75*, 4560-2.
45. Nave, S. E.; Haire, R. G.; Huray, P. G., Magnetic properties of actinide elements having the 5f6 and 5f7 electronic configurations. *Phys. Rev. B: Condens. Matter* **1983,** *28* (5), 2317-27.
46. Noe, M.; Fuger, J.; Duyckaerts, G., Recent observations on curium sesquioxide. *Inorg. Nucl. Chem. Lett.* **1970,** *6* (1), 111-19.
47. Baybarz, R. D., High-temperature phases, crystal structures, and melting points for transplutonium sesquioxides. *J. Inorg. Nucl. Chem.* **1973,** *35* (12), 4149-58.
48. Haire, R. G.; Baybarz, R. D., Identification and analysis of einsteinium sesquioxide by electron diffraction. *J. Inorg. Nucl. Chem.* **1973,** *35* (2), 489-96.
49. Haschke, J. M.; Allen, T. H.; Morales, L. A., Surface and corrosion chemistry of plutonium. *Los Alamos Sci.* **2000,** *26* (Vol. 1), 252-273.
50. (a) Prodan, I. D.; Scuseria, G. E.; Sordo, J. A.; Kudin, K. N.; Martin, R. L., Lattice defects and magnetic ordering in plutonium oxides: A hybrid density-functional-theory study of strongly correlated materials. *The Journal of Chemical Physics* **2005,** *123* (1), 014703; (b) Atta-Fynn, R.; Ray, A. K., Bulk and (11$\bar{2}$0) surface properties of β-Pu2O3: A theoretical study using DFT with exact exchange for correlated electrons. *Chem. Phys. Lett.* **2013,** *583*, 42-48; (c) Ao, B.; Qiu, R.; Lu, H.; Chen, P., First-principles DFT + U calculations on the energetics of Ga in Pu, Pu2O3 and PuO2. *Comput. Mater. Sci.* **2016,** *122*, 263-271; (d) Sun, B.; Zhang, P.; Zhao, X.-G., First-principles local density approximation + U and generalized gradient approximation + U study of plutonium oxides. *J. Chem. Phys.* **2008,** *128* (8), 084705/1-084705/7; (e) Sun, B.; Zhang, P.; Zhao, X.-G., First-principles local density approximation + U and generalized gradient approximation + U study of plutonium oxides. [Erratum to document cited in CA148:387899]. *J. Chem. Phys.* **2009,** *131* (16), 169903/1; (f) Jomard, G.; Amadon, B.; Bottin, F.; Torrent, M., Structural, thermodynamic, and electronic properties of plutonium oxides from first principles. *Phys. Rev. B: Condens. Matter Mater. Phys.* **2008,** *78* (7), 075125/1-075125/11.
51. Amadon, B., A self-consistent DFT + DMFT scheme in the projector augmented wave method: applications to cerium, Ce2O3 and Pu2O3 with the Hubbard I solver and comparison to DFT + U. *J. Phys.: Condens. Matter* **2012,** *24* (7), 075604/1-075604/13.
52. (a) Lu, Y.; Yang, Y.; Zheng, F.; Zhang, P., Phonon dispersion curves and thermodynamic properties of α-Pu2O3. *arXiv.org, e-Print Arch., Condens. Matter* **2012**, 1-6, arXiv:1208.3746v1 [cond-mat.mtrl-sci]; (b) Sun, B.; Liu, H.; Song, H.; Zhang, G.; Zheng, H.; Zhao, X.; Zhang, P., The environmental dependence of redox energetics of PuO2 and α-Pu2O3: A quantitative solution from DFT+U. *Phys. Lett. A*

2012, *376* (40-41), 2672-2676; (c) Yang, Y.; Lu, Y.; Zhang, P., Optical properties of PuO2 and α-Pu2O3 by GGA + U + QA studies. *J. Nucl. Mater.* **2014,** *452* (1-3), 414-418.
53. Zachariasen, W. H. CK-1367; 1944.
54. Suzuki, C.; Nishi, T.; Nakada, M.; Tsuru, T.; Akabori, M.; Hirata, M.; Kaji, Y., DFT study on the electronic structure and chemical state of Americium in an (Am,U) mixed oxide. *J. Phys. Chem. Solids* **2013,** *74* (12), 1769-1774.
55. Wen, X.-D.; Martin, R. L.; Scuseria, G. E.; Rudin, S. P.; Batista, E. R., A Screened Hybrid DFT Study of Actinide Oxides, Nitrides, and Carbides. *The Journal of Physical Chemistry C* **2013,** *117* (25), 13122-13128.
56. Desgranges, L.; Baldinozzi, G.; Simeone, D.; Fischer, H. E., Refinement of the α-U4O9 Crystalline Structure: New Insight into the U4O9 → U3O8 Transformation. *Inorg. Chem.* **2011,** *50* (13), 6146-6151.
57. Desgranges, L.; Baldinozzi, G.; Rousseau, G.; Niepce, J.-C.; Calvarin, G., Neutron Diffraction Study of the in Situ Oxidation of UO2. *Inorg. Chem.* **2009,** *48* (16), 7585-7592.
58. Garrido, F.; Ibberson, R. M.; Nowicki, L.; Willis, B. T. M., Cuboctahedral oxygen clusters in U3O7. *J. Nucl. Mater.* **2003,** *322* (1), 87-89.
59. Hoekstra, H. R.; Siegel, S.; Gallagher, F. X., Uranium-oxygen system at high pressure. *J. Inorg. Nucl. Chem.* **1970,** *32* (10), 3237-48.
60. Hoekstra, H.; Siegel, S.; Charpin, P., The synthesis of UO2·37 at high pressure. *Journal of Inorganic and Nuclear Chemistry* **1968,** *30* (2), 519-523.
61. Forbes, T. Z.; Burns, P. C.; Skanthakumar, S.; Soderholm, L., Synthesis, Structure, and Magnetism of Np2O5. *J. Am. Chem. Soc.* **2007,** *129* (10), 2760-2761.
62. Andersen, A. F., The structure of U3O8 determined by neutron diffraction. *Acta Crystallogr.* **1958,** *11*, 612-14.
63. Chodura, B.; Maly, J., Determination of the structure of U3O8. *Proc. U. N. Int. Conf. Peaceful Uses At. Energy, 2nd* **1958,** *28*, 223-30.
64. Colmenares, C. A., The oxidation of thorium, uranium, and plutonium. *Prog. Solid State Chem.* **1975,** *9*, 139-239.
65. Zachariasen, W. H., Crystal chemical studies of the 5 f-series of elements. I. New structure types. *Acta Crystallogr.* **1948,** *1*, 265-8.
66. Loopstra, B. O.; Cordfunke, E. H. P., Structure of α-UO3. *Recl. Trav. Chim. Pays-Bas* **1966,** *85* (2), 135-42.
67. Debets, P. C., The structure of β-UO3. *Acta Crystallogr.* **1966,** *21* (4), 589-93.
68. Loopstra, B. O.; Taylor, J. C.; Waugh, A. B., Neutron powder profile studies of the gamma uranium trioxide phases. *J. Solid State Chem.* **1977,** *20* (1), 9-19.
69. Weller, M. T.; Dickens, P. G.; Penny, D. J., The structure of δ-uranium trioxide. *Polyhedron* **1988,** *7* (3), 243-4.
70. Siegel, S.; Hoekstra, H.; Sherry, E., The crystal structure of high-pressure UO3. *Acta Crystallogr.* **1966,** *20* (2), 292-5.
71. Andersson, D. A.; Lezama, J.; Uberuaga, B. P.; Deo, C.; Conradson, S. D., Cooperativity among defect sites in AO2+x and A4O9 (A=U,Np,Pu): Density functional calculations. *Phys. Rev. B: Condens. Matter Mater. Phys.* **2009,** *79* (2), 024110/1-024110/12.
72. He, H.; Andersson, D. A.; Allred, D. D.; Rector, K. D., Determination of the Insulation Gap of Uranium Oxides by Spectroscopic Ellipsometry and Density Functional Theory. *The Journal of Physical Chemistry C* **2013,** *117* (32), 16540-16551.
73. Andersson, D. A.; Baldinozzi, G.; Desgranges, L.; Conradson, D. R.; Conradson, S. D., Density Functional Theory Calculations of UO2 Oxidation: Evolution of UO2+x, U4O9–y, U3O7, and U3O8. *Inorganic Chemistry* **2013,** *52* (5), 2769-2778.

74. Brincat, N. A.; Molinari, M.; Parker, S. C.; Allen, G. C.; Storr, M. T., Computer simulation of defect clusters in UO2 and their dependence on composition. *Journal of Nuclear Materials* **2015,** *456*, 329-333.
75. Brincat, N. A.; Molinari, M.; Allen, G. C.; Storr, M. T.; Parker, S. C., Density functional theory calculations of defective UO2 at U3O7 stoichiometry. *Journal of Nuclear Materials* **2015,** *467*, 724-729.
76. (a) Pireaux, J. J.; Riga, J.; Thibaut, E.; Tenret-Noel, C.; Caudano, R.; Verbist, J. J., Shake-up satellites in the x-ray photoelectron spectra of uranium oxides and fluorides. A band structure scheme for uranium dioxide, UO2. *Chem. Phys.* **1977,** *22* (1), 113-20; (b) Teterin, Y. A.; Teterin, A. Y., The structure of X-ray photoelectron spectra of light actinide compounds. *Russ. Chem. Rev.* **2004,** *73* (6), 541-580.
77. Brincat, N. A.; Parker, S. C.; Molinari, M.; Allen, G. C.; Storr, M. T., Density functional theory investigation of the layered uranium oxides U3O8 and U2O5. *Dalton Trans.* **2015,** *44* (6), 2613-2622.
78. Molinari, M.; Brincat, N. A.; Allen, G. C.; Parker, S. C., Structure and Properties of Some Layered U2O5 Phases: A Density Functional Theory Study. *Inorg. Chem.* **2017,** *56* (8), 4469-4474.
79. Yun, Y.; Rusz, J.; Suzuki, M. T.; Oppeneer, P. M., First-principles investigation of higher oxides of uranium and neptunium: ${\mathrm{U}}_{3}$O${}_{8}$ and Np${}_{2}$O${}_{5}$. *Physical Review B* **2011,** *83* (7), 075109.
80. Xiao-Dong, W.; Richard, L. M.; Gustavo, E. S.; Sven, P. R.; Enrique, R. B.; Anthony, K. B., Screened hybrid andDFT + U studies of the structural, electronic, and optical properties of U 3 O 8. *Journal of Physics: Condensed Matter* **2013,** *25* (2), 025501.
81. Geng, H. Y.; Song, H. X.; Jin, K.; Xiang, S. K.; Wu, Q., First-principles study on oxidation effects in uranium oxides and high-pressure high-temperature behavior of point defects in uranium dioxide. *Physical Review B* **2011,** *84* (17), 174115.
82. Brincat, N. A.; Parker, S. C.; Molinari, M.; Allen, G. C.; Storr, M. T., Ab Initio Investigation of the UO3 Polymorphs: Structural Properties and Thermodynamic Stability. *Inorg. Chem.* **2014,** *53* (23), 12253-12264.
83. Idriss, H., Surface reactions of uranium oxide powder, thin films and single crystals. *Surf. Sci. Rep.* **2010,** *65* (3), 67-109.
84. Meredig, B.; Agrawal, A.; Kirklin, S.; Saal, J. E.; Doak, J. W.; Thompson, A.; Zhang, K.; Choudhary, A.; Wolverton, C., Combinatorial screening for new materials in unconstrained composition space with machine learning. *Physical Review B* **2014,** *89* (9), 094104.
85. Allen, J. P.; Watson, G. W., Occupation matrix control of d- and f-electron localisations using DFT + U. *Physical Chemistry Chemical Physics* **2014,** *16* (39), 21016-21031.
86. Claisse, A.; Klipfel, M.; Lindbom, N.; Freyss, M.; Olsson, P., GGA+U study of uranium mononitride: A comparison of the U-ramping and occupation matrix schemes and incorporation energies of fission products. *Journal of Nuclear Materials* **2016,** *478*, 119-124.